AD-A084 738 TEXAS UNIV AT AUSTIN APPLIED RESEARCH LABS F/G 20/1
SEDIMENT ACOUSTICS.(U)
APR 80 D J SHIRLEY, J M HOVEM, G D INGRAM N00014-76-C-0117
UNCLASSIFIED ARL-TR-80-17 NL

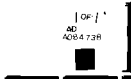

END
DATE FILMED
6-80
DTIC

ARL-TR-80-17

SEDIMENT ACOUSTICS

Annual Report under Contract N00014-75-C-0117

Donald J. Shirley
Jens M. Hovem
Greg D. Ingram
David W. Bell

APPLIED RESEARCH LABORATORIES
THE UNIVERSITY OF TEXAS AT AUSTIN
POST OFFICE BOX 8029, AUSTIN, TEXAS 78712

2 April 1980

Technical Report

1 January - 31 December 1979

Prepared for:

OFFICE OF NAVAL RESEARCH
DEPARTMENT OF THE NAVY
ARLINGTON, VA 22217

UNCLASSIFIED

SECURITY CLASSIFICATION OF THIS PAGE *(When Data Entered)*

REPORT DOCUMENTATION PAGE

READ INSTRUCTIONS BEFORE COMPLETING FORM

1. REPORT NUMBER	2. GOVT ACCESSION NO. AD-A084 738
3. RECIPIENT'S CATALOG NUMBER	
4. TITLE *(and Subtitle)* SEDIMENT ACOUSTICS	5. TYPE OF REPORT & PERIOD COVERED annual report 1 January - 31 December 1979
6. PERFORMING ORG. REPORT NUMBER ARL-TR-80-17	
7. AUTHOR(s) Donald J. Shirley, Jens M. Hovem, Greg D. Ingram, David W. Bell	8. CONTRACT OR GRANT NUMBER(s) N00014-76-C-0117
9. PERFORMING ORGANIZATION NAME AND ADDRESS Applied Research Laboratories The University of Texas at Austin Austin, TX 78712	10. PROGRAM ELEMENT, PROJECT, TASK AREA & WORK UNIT NUMBERS
11. CONTROLLING OFFICE NAME AND ADDRESS Office of Naval Research Department of the Navy Arlington, VA 22217	12. REPORT DATE 2 Apr 80
	13. NUMBER OF PAGES 91
14. MONITORING AGENCY NAME & ADDRESS(if different from Controlling Office) 1 Jan-31 Dec 79	15. SECURITY CLASS. *(of this report)* UNCLASSIFIED
	15a. DECLASSIFICATION/DOWNGRADING SCHEDULE N/A

16. DISTRIBUTION STATEMENT *(of this Report)*

Approved for public release; distribution unlimited.

17. DISTRIBUTION STATEMENT *(of the abstract entered in Block 20, if different from Report)*

18. SUPPLEMENTARY NOTES

19. KEY WORDS *(Continue on reverse side if necessary and identify by block number)*

in situ
acoustics
sediments
shear wave
compressional wave

20. ABSTRACT *(Continue on reverse side if necessary and identify by block number)*

(U) During the period 1 January - 31 December 1979, work under Contract N00014-76-C-0117 consisted of three parts: (1) use of the profilometer system to obtain in situ compressional wave data and to test in situ shear wave transducers, (2) development of theoretical models for acoustic propagation in sediments, and (3) laboratory measurements of compressional wave and shear wave parameters in laboratory sediments. Data obtained for the three parts of the program are reported.

DD FORM 1 JAN 73 1473 EDITION OF 1 NOV 65 IS OBSOLETE

UNCLASSIFIED

SECURITY CLASSIFICATION OF THIS PAGE *(When Data Entered)*

1/04 454

TABLE OF CONTENTS

LIST OF FIGURES

I. INTRODUCTION

A determination of the viscoelastic properties of ocean sediments can be made by measurement of the compressional wave and shear wave speeds, the compressional wave and shear wave attenuations, and acoustic impedance.[1] The measurements can be made in either of two ways: (1) in situ measurements with instruments in place in the natural environment provide better data due to decreased disturbance of the medium, but at the same time are more costly, less controlled, and are more difficult to perform; (2) laboratory measurements made on samples of the sediment retrieved from the bottom are by necessity conducted on material that is disturbed by the sampling and retrieval process, and if not made immediately after retrieval, the measurements are further degraded by dehydration and disturbance during storage.

The best program for measuring the acoustic properties of ocean bottom sediments is one which obtains the data in situ with methods and equipment that minimize the expense of doing so.

For the past several years Applied Research Laboratories, The University of Texas at Austin (ARL:UT), has had a program funded by the Office of Naval Research (ONR) to develop the capability of measuring compressional wave, shear wave, and acoustic impedance properties of marine sediments in situ. The capability of making laboratory measurements of acoustical parameters and physical properties to augment and support the goal of in situ measurements has developed from the program. One major result has been development of an instrument to obtain a profile of sediment acoustic properties during routine coring. The measurements are made by attaching self-contained instrumentation to existing coring equipment. Measurement and recording circuits contained in a pressure case are attached to the top weighted end of a corer. Appropriate transducers are

attached to the cutter at the bottom of the core barrel and are connected to the instrumentation case by cables running along the outside of the core barrel. The unit is used during normal coring operations, and adds little time or effort to the procedure.[2]

This profilometer system has developed in stages up to the present time and certain aspects of it are still under development. In 1971, the feasibility of such measurements was demonstrated using laboratory equipment and a small mud tank.[3] Once feasibility was demonstrated, equipment was built to allow field measurements using a piston corer and a hand corer in shallow water with cables to the surface.[4] In 1974, the profilometer was redesigned so that the recording and measuring system was contained in a pressure case to eliminate the problems associated with cables to the surface.[5] The success of the compressional wave measurements prompted an investigation into the possibility of adding shear wave and acoustic impedance measurements to the system; this was begun in 1975.[6] Shear wave transducer design has now progressed to the point that field tests have been made.[7] During development of the in situ measurement capability, an extensive program of laboratory acoustical measurements in both natural and artificial sediments was also in progress using the new transducers developed for the in situ work.[8] Development work on measurement of acoustic impedance has produced a transducer design suitable for use in the profilometer system.[9]

During 1979, the project was divided into three major parts; these are described in this report.

(1) Use of the profilometer equipment in the field to make compressional wave measurements in situ and to test shear wave transducer designs.
(2) Design and development of in situ shear wave transducers.
(3) Theoretical and laboratory experimental work to develop models for acoustic propagation in sediments.

A bibliography of publications under the sediment acoustics program is included in this report as Appendix A. During the past several years,

13 technical reports have been published, 13 papers have been presented at technical meetings, 7 papers have been published in scientific journals, 3 papers have been included in books, and 2 invention disclosures have been submitted for patent. Of these, 3 publications and 2 technical reports were issued and 3 papers were presented during 1979.[10-17]

II. FIELD MEASUREMENTS

A. Introduction

During 1979, three field trips aboard ship were conducted to record compressional wave data and to evaluate in situ shear wave transducer designs. The first trip was aboard USNS BARTLETT (T-AGOR 13) in the Caribbean Sea. Two corings were attempted with the newly designed and constructed profilometer equipment but design problems caused the equipment to malfunction. Although the equipment was altered and the problem corrected, the ship broke down and the cruise was aborted. Thus, no valid compressional wave data were obtained and the shear wave transducers were not tested. The second trip was aboard R/V IDA GREEN in the Gulf of Mexico. Five profiles were successfully obtained, one of which was a successful test of a shear wave transducer design. The third trip, aboard R/V GYRE (AGOR 21), was a substitute for the aborted cruise aboard USNS BARTLETT. Several equipment malfunctions caused the loss of some data but one good compressional wave profile was obtained during this trip. The data from the R/V IDA GREEN and R/V GYRE cruises will be described in detail below.

B. R/V IDA GREEN Cruise

A field trip aboard R/V IDA GREEN, operated by The University of Texas Marine Science Institute (MSI), was conducted during the period 7-12 August 1979. Six cores were obtained from the northern Gulf of Mexico; these sites are shown on a map of the operating area, Fig. 1. The profilometer was attached to the corer for all six corings. Four compressional wave profiles were obtained out of five attempts. On the last core, the transducer was slightly damaged when the corer penetrated a hard shell layer

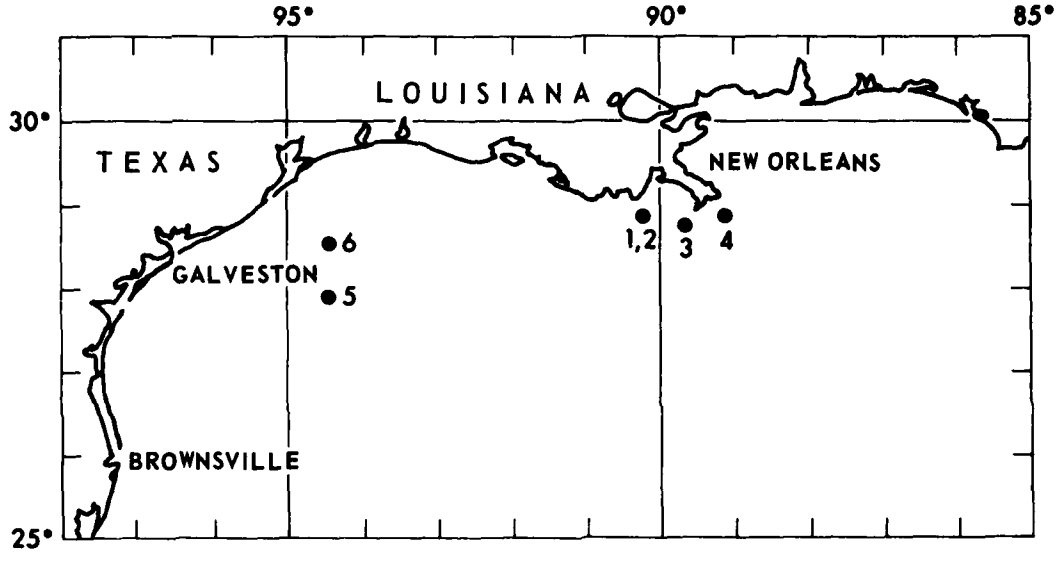

FIGURE 1
CORE LOCATIONS
R/V IDA GREEN CRUISE
AUGUST 1979

ARL:UT
AS-80-941
DJS-GA
3-21-80

and no valid data were obtained. For core 2 the profilometer was set up to record shear wave parameters using a new transducer design.

Figures 2-5 show the compressional wave profiles obtained for cores 1, 3, 4, and 5, respectively. The top trace in each figure is the compressional wave speed profile, the middle trace is pulse amplitude, which provides a measure of the loss of the acoustic wave propagating through the sediment, and the bottom trace is a profile of the acceleration experienced by the corer. The horizontal axis represents depth in the bottom derived from a double integration of the acceleration. The sediment-water interface is at zero on the horizontal axis, and depth into the bottom increases to the right. Negative numbers on the axis indicate the part of the profile obtained in the overlying water.

Core 1 was obtained in 15 m of water near the mouth of the Mississippi River as indicated on the map of Fig. 1. The sound speed and amplitude profiles are similar to others made in shallow water with a bottom composed of sand and mud.[18] The sound speed profile has an initial large gradient of about 160 sec^{-1}, and then levels off near 1900 m/sec for approximately 1 m, after which it decreases very sharply. The sharp drop occurs at a point where the signal level decreases to less than the detection threshold for the instrument (-20 dB), which indicates that the data at this point is not valid. The level areas on both the sound speed and amplitude profiles are saturation levels for the plotting system and do not represent valid measurements. The large decrease in amplitude could possibly be due to gas in the sediment which would cause large attenuation of the acoustic signal. The rough and variable nature of the acceleration profile indicates that the corer penetrated a bottom composed of several layers of varying stiffness.

Core 3 was the next core made with the compressional wave equipment; it was also on the Mississippi Delta several kilometers distant from core 1. The water depth at the core 3 location was somewhat deeper (64 m) and the bottom characteristics were much different--soft mud as opposed to sandy mud. Hence the profiles for core 1 and core 3 are considerably

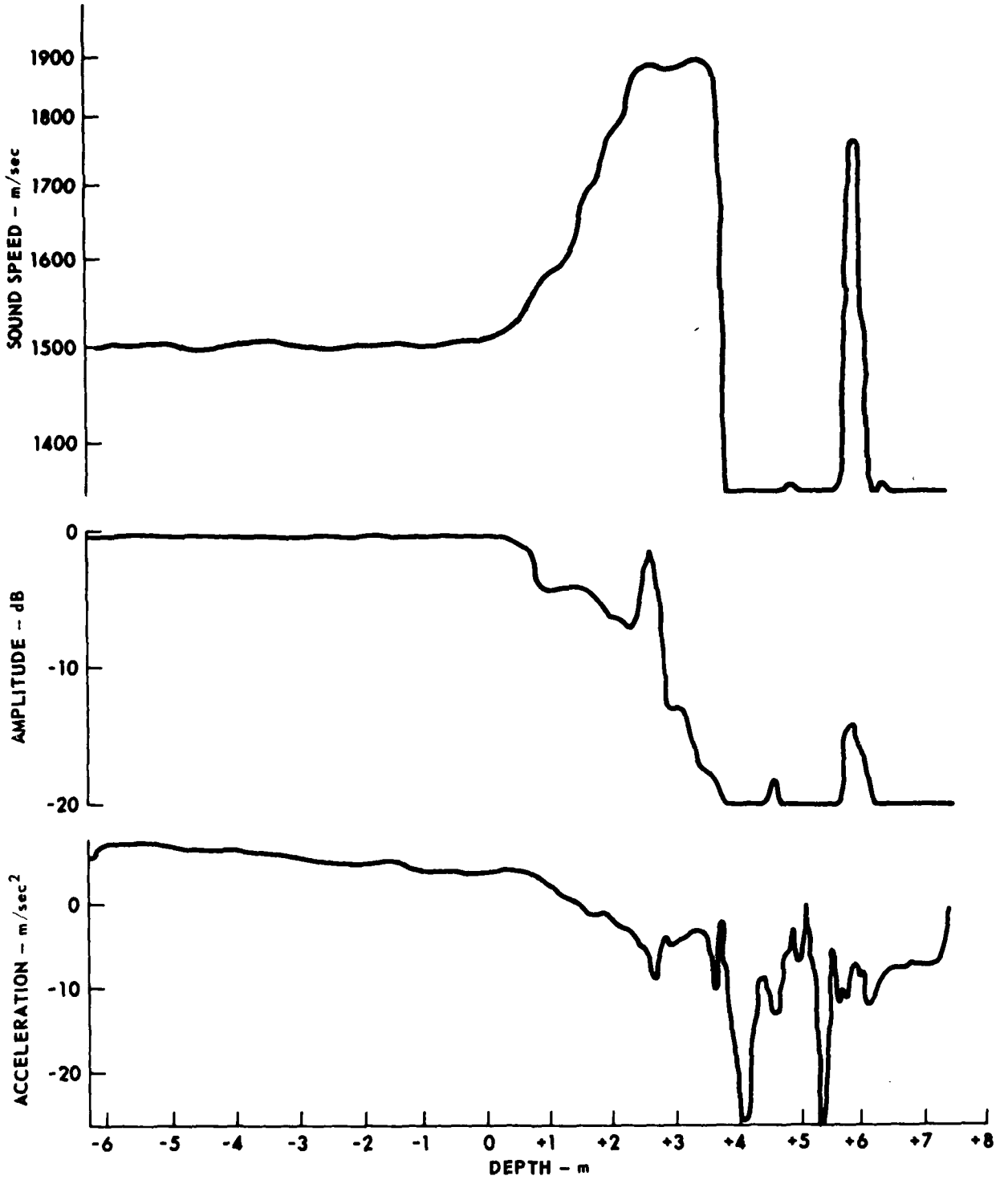

FIGURE 2
COMPRESSIONAL WAVE PROFILES FOR CORE 1
R/V IDA GREEN

ARL:UT
AS-80-942
DJS-GA
3-21-80

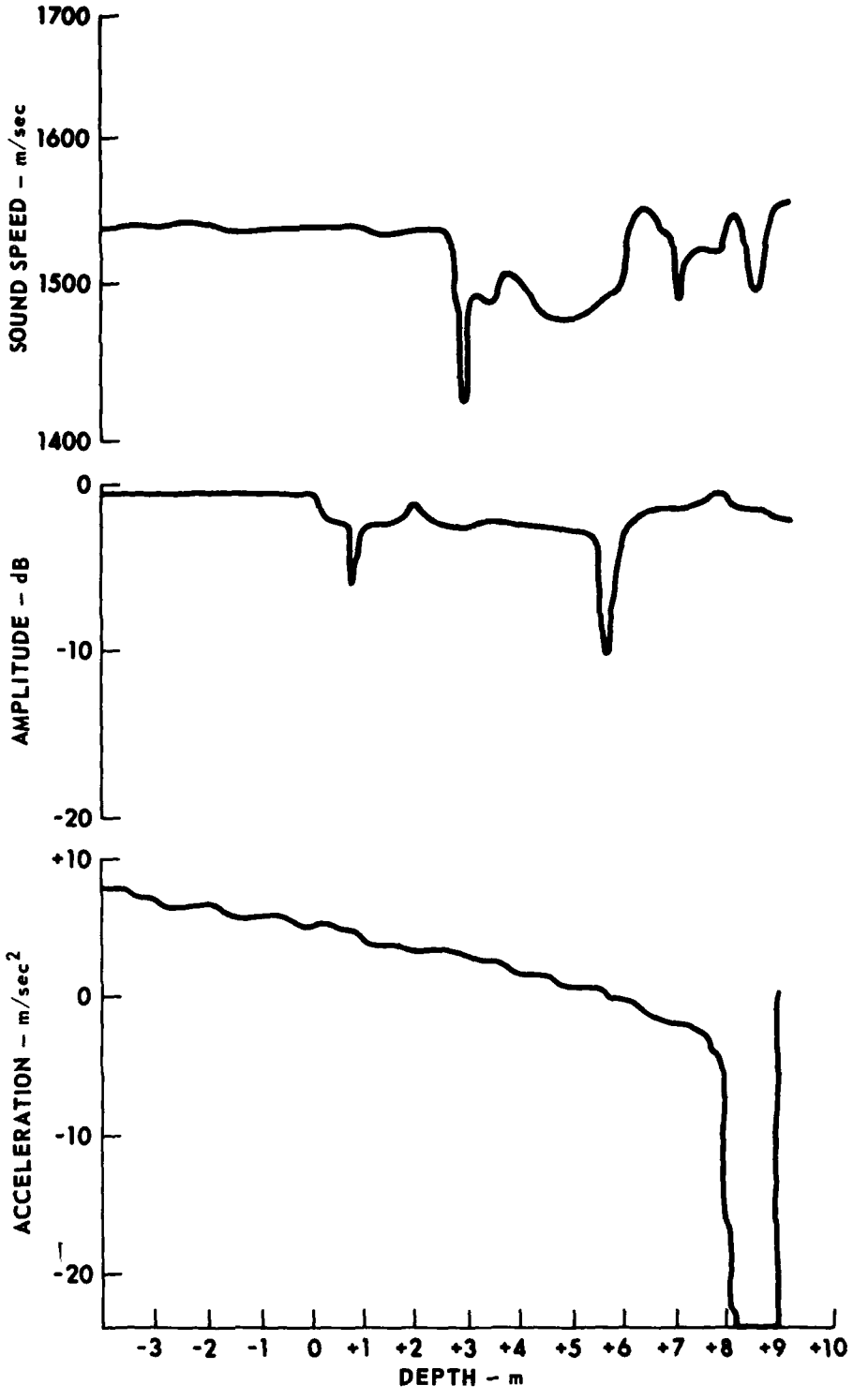

FIGURE 3
COMPRESSIONAL WAVE PROFILES FOR CORE 3
R/V IDA GREEN

ARL:UT
AS-80-943
DJS-GA
3-21-80

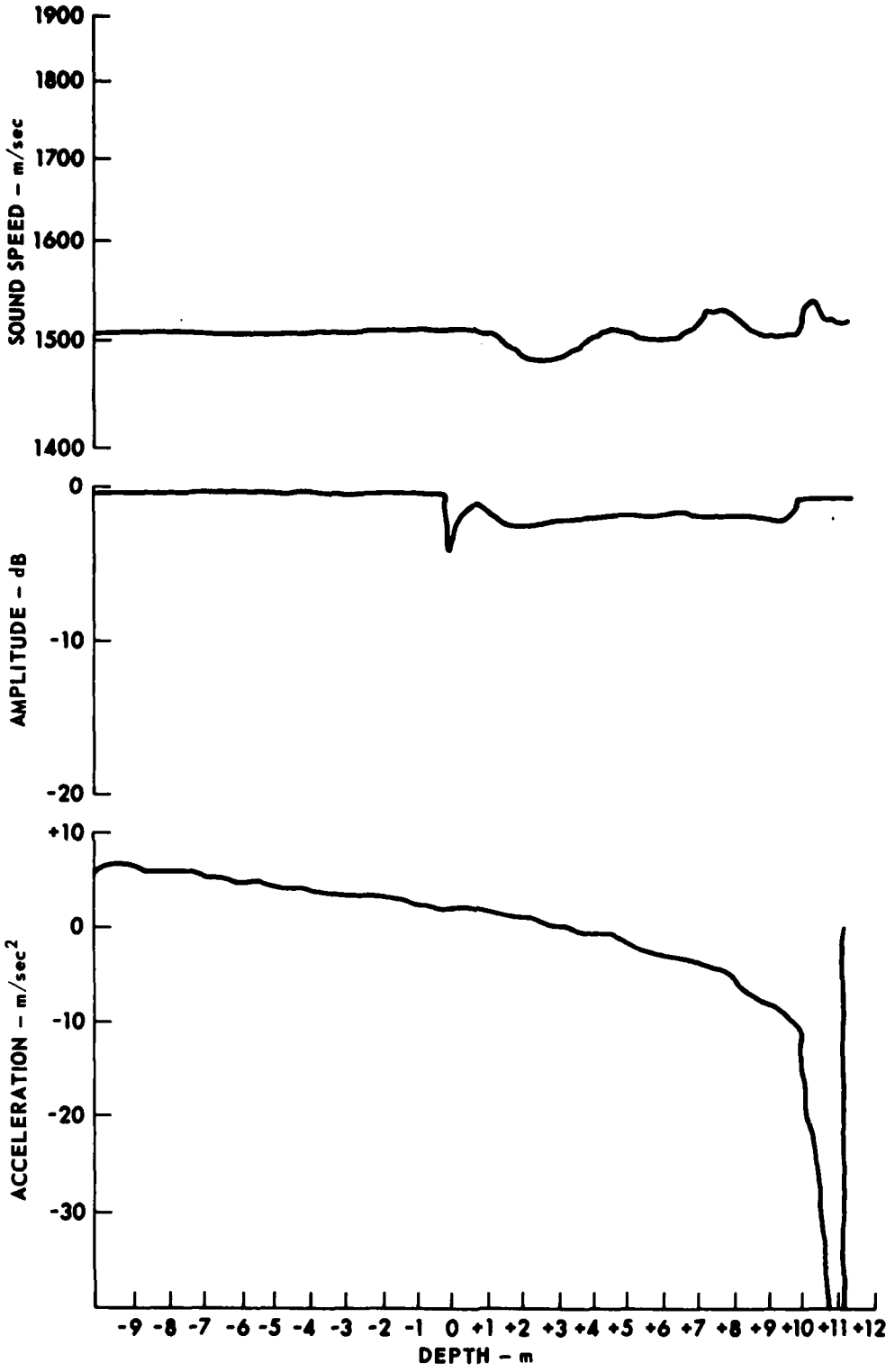

FIGURE 4
COMPRESSIONAL WAVE PROFILES FOR CORE 4
R/V IDA GREEN

ARL:UT
AS-80-944
DJS-GA
3-21-80

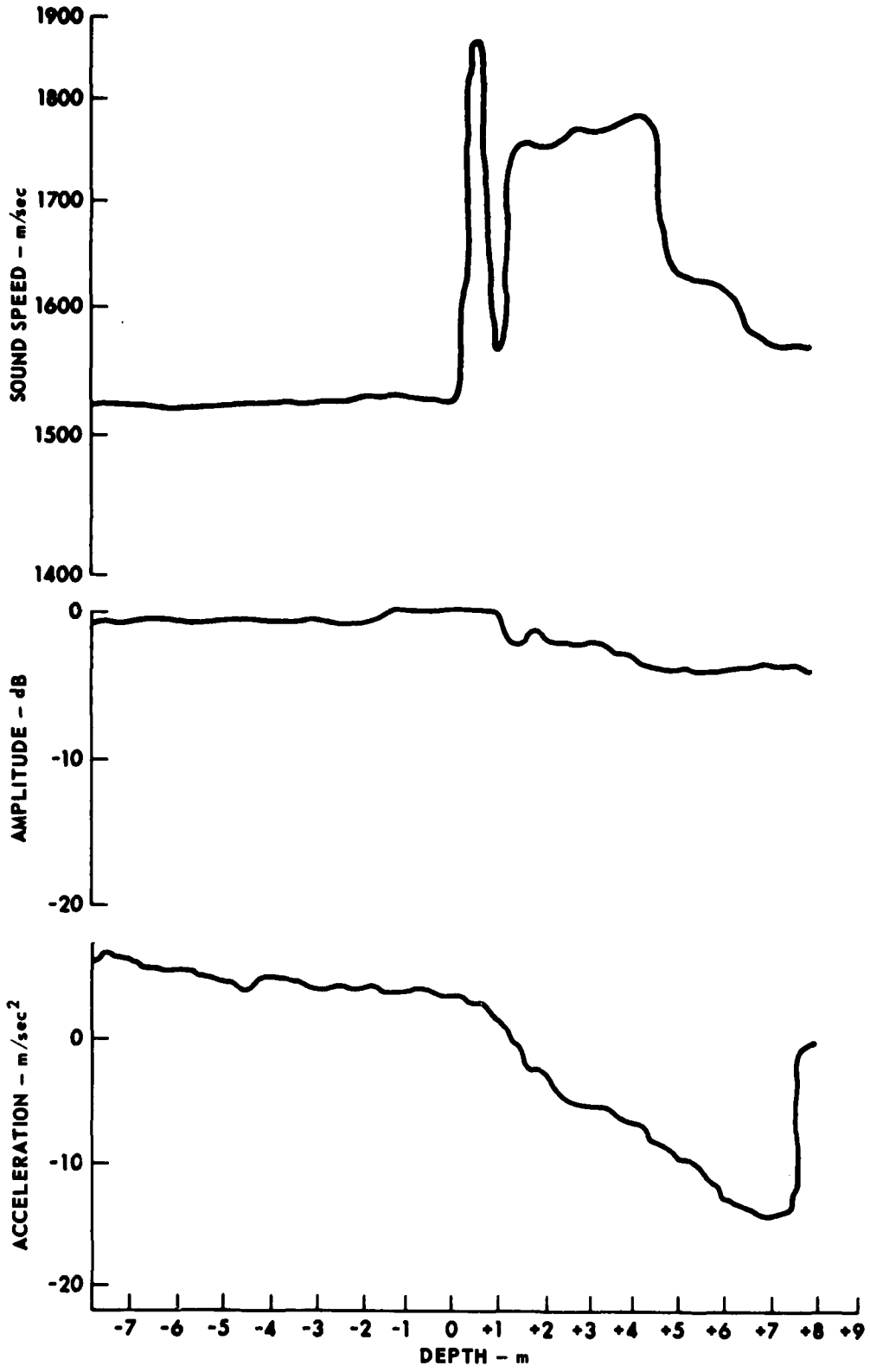

FIGURE 5
COMPRESSIONAL WAVE PROFILES FOR CORE 5
R/V IDA GREEN

ARL:UT
AS-80-945
DJS-GA
3-21-80

different. In core 3 the sound speed in sediment is generally lower than in the overlying water, but with some variability. There is also much less attenuation in the sediment. The smoothness of the acceleration trace indicates that the bottom was soft and homogeneous. The sudden large decrease in the acceleration profile at the end is more likely due to the core barrel becoming plugged with sediment rather than from a hard sediment layer being encountered.

Core 4 was made a few kilometers from core 3 and is very similar to core 3.

Core 5 was obtained just off the Texas coast near Galveston in 97 m of water and shows a compressional wave speed profile similar to that of core 1. In the case of core 5, the attenuation is less than that encountered in core 1, and this reduced attenuation resulted in a more complete sound speed profile.

One purpose of the field trip aboard R/V IDA GREEN was to test a new in situ shear wave transducer design. The new design, illustrated in Fig. 6, consists of an outrigger arrangement attached to the core cutter in a manner similar to the normal transducer arrangement, but with the active elements extending ahead of the cutting edge. Single ceramic bender elements similar to those that have been described for laboratory measurements[19] are attached to the outrigger so that shear waves can be generated and detected out in front of the corer. This design allows total contact of the shear wave element with the sediment, which in turn enhances the amount of shear wave energy coupled into and out of the sediment over that of previous designs.[7,13] Previous designs had failed to function satisfactorily due to the low signal-to-noise ratio (S/N) while the corer was moving and generating shear wave noise. Also, the shear wave pressure release material (i.e., a fluid filling around the element array) used in the older design tended to be subject to damage and leakage.[7,13] By installing a single shear wave element coated with a thin plastic waterproof sheath, the above two problems could be eliminated.

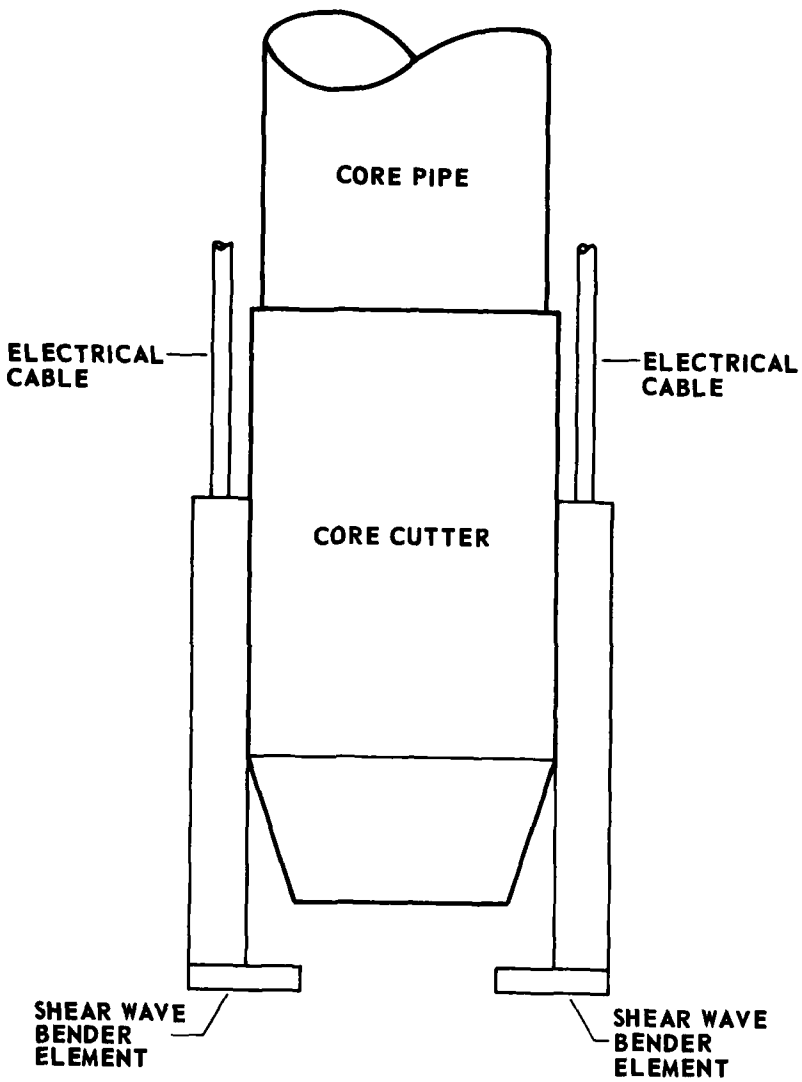

FIGURE 6
SHEAR WAVE TRANSDUCER ARRANGEMENT ON CORER

ARL:UT
AS-80-946
DJS-GA
3-21-80

Since the new design transducer projects out in front of the core cutter, there is a high probability of damage to the transducer if a hard material is penetrated by the corer. Within the operating area of the R/V IDA GREEN the soft muds of the Mississippi Delta were thought to provide the least likelihood of transducer damage. A site was picked (core 2) which was in an area of sandy mud exhibiting relatively high compressional wave speed (see core 1), but which could be easily penetrated and had no hard layers. The sandy mud sediment should have relatively higher shear wave speed and lower shear wave attenuation compared to softer muds and clays.

Figure 7 shows the shear wave profiles obtained for core 2. The top trace is the shear wave speed and the bottom trace is the acceleration profile. Due to a malfunction, no amplitude data were obtained for this core. Unfortunately a bed of shell was penetrated by the corer and the shear wave transducers were damaged after penetration to about 5 m.

There are some features of the in situ shear wave speed profile for core 2 which tend to degrade the quality of the shear wave data and which need to be examined carefully before pronouncing the test a success.

The first such feature is the part of the profile where the transducers are still in the water above the bottom--the part from the beginning to the point marked B. Penetration into the bottom is indicated at point B by the change in the acceleration profile. The water column data can further be divided into the areas from the beginning to point A and from A to B.

The nature of shear waves prohibits their propagation in a fluid such as water so that the data indicated on the shear wave speed profile to point B is not due to shear wave propagation. In laboratory tests it was observed that when the transducers were immersed in a fluid such as air or water, there was a significant amount of energy transmitted through the transducer mounts and cutter with a delay such as to appear in the receiver as a fast (approximately 400 m/sec) shear wave. It was also observed that the feed-around signal decreased to an immeasurable level when the shear

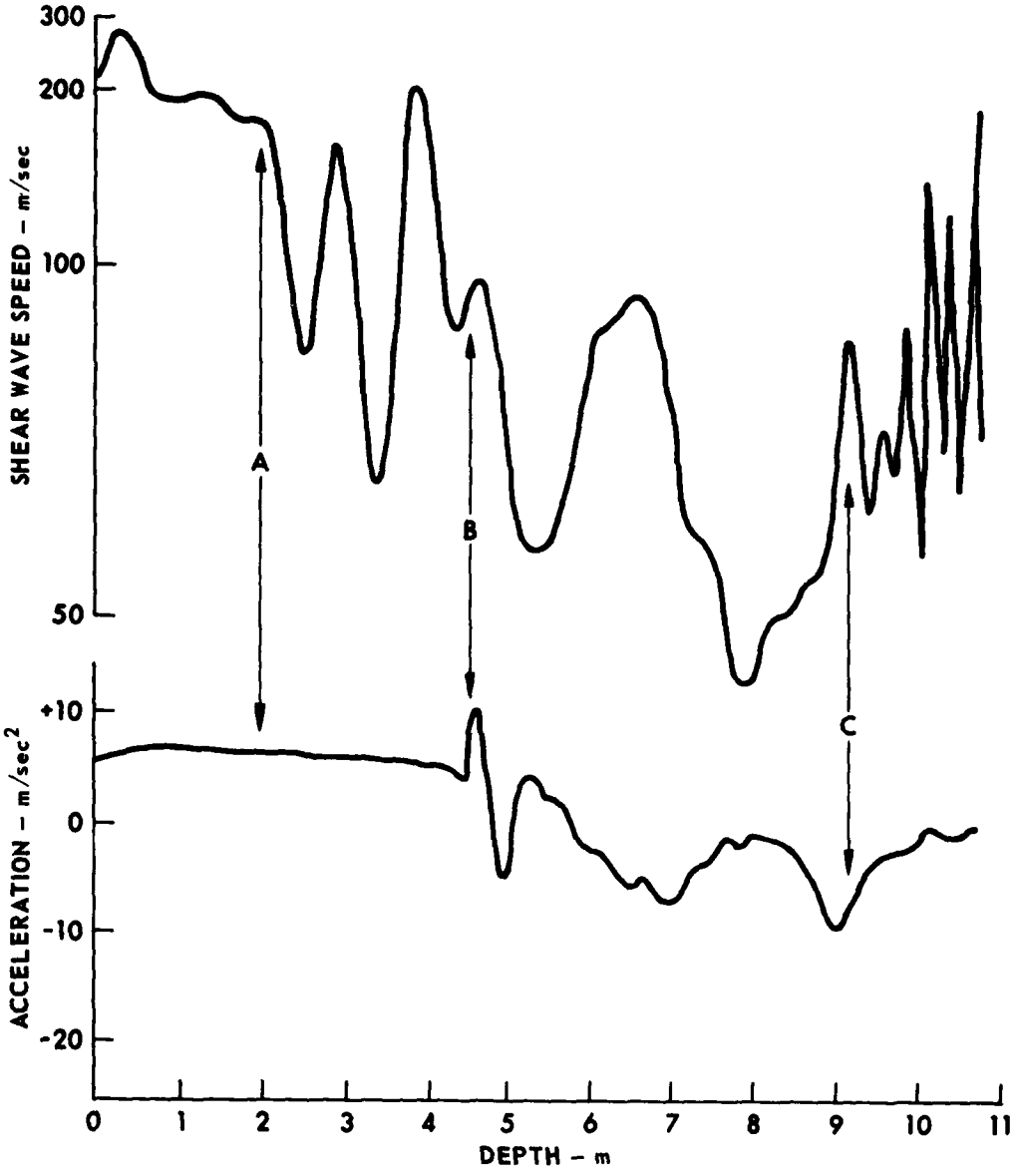

FIGURE 7
SHEAR WAVE PROFILES FOR CORE 2
R/V IDA GREEN

ARL:UT
AS-80-947
DJS-GA
3-21-80

wave transducers were inserted into a sediment. The decrease is due to the fact that while in contact with a solid such as a sediment, most of the acoustic energy generated by the transducer is propagated as shear waves and so is not available for a feed-around compressional wave signal. The profilometer detection threshold is normally set low enough that the feed-around signal is detected so it was expected that the shear wave profile would exhibit a constant high speed during the time the transducers were in the water overlying the bottom.

The reason for the large oscillations in the shear wave speed profile between point A and point B is at present unknown. On the type of corer that was utilized for the test, a piston is attached to the end of the corer suspension cable and is set so that the piston starts moving up the inside of the core barrel at the moment the cutter first enters the bottom. If in fact the cable length was not set accurately and the piston started moving above the bottom, the resulting noise generated by the moving piston could interact with the feed-around signal to produce such an artifact on the profile. There is no easy way of testing the above hypothesis in the laboratory so resolution of the problem must await further field testing of the shear wave transducers.

The portion of the profile between points B and C is what could be expected for a shear wave in the type of sediment encountered. The sudden change in the acceleration profile at point B indicates that the corer entered the bottom. As the bottom is penetrated, the acceleration profile indicates that several layers of varying stiffness and shear strength occur. An increase in acceleration in the positive direction indicates reduced shear strength. A sediment with increasing shear strength should show an equivalent increase in shear wave speed. The changes in shear wave speed indicated by the speed profile do indeed show good correlation with the changes in the acceleration profile. The point marked C on the acceleration record indicates a fairly thin hard layer has been encountered; it was probably at this point that the shear wave transducer was destroyed. Also at point C, the shear wave speed record shows a definite change in the profile with the variations becoming short and seemingly random, which

indicates that the measuring circuits are not locked onto a received pulse.

Although the profile is not clear and contains some unexplainable features, there is a good probability that the instrument did measure the in situ shear wave speed for part of its penetration.

C. R/V GYRE Cruise

During the period 7-26 November 1979, a field trip with Naval Ocean Research and Development Activity (NORDA) personnel aboard R/V GYRE was conducted in the Caribbean Sea. Nine piston cores were made; the profilometer was attached to the corer for five of them. Only one good compressional wave profile was obtained due to several mishaps during deployment of the corer in rough seas and to malfunctioning of the profilometer tape recorder mechanism. Tests on the shear wave transducers were not completed because the coring winch failed after core 9 was obtained, which stopped piston coring operations for the remainder of the cruise.

The one good profile obtained during the trip is shown in Fig. 8. Location of the core was in the Venezuelan Basin near the Aves Ridge at latitude 12°59.4'N and longitude 65°27.8'W at 4480 m water depth. This profile is one of the most informative compressional wave profiles obtained with the profilometer. The corer penetrated 13 m, which is the full length of the core barrels, and a core of 12.26 m length was retained. This small differential between penetration and core length is seen in the profiles in Fig. 8. At a depth of a little over 11 m, the amplitude and speed profiles became constant, indicating that sediment was no longer entering the core cutter. The plugged condition is also indicated by the sudden increase in deceleration seen at this point on the acceleration profile, which is due to the greater resistance to penetration of the plugged core barrels.

The compressional wave speed profile indicates that the speed in the bottom is higher than the speed in the overlying water with several interleaved layers with lower speeds toward the middle of the profile.

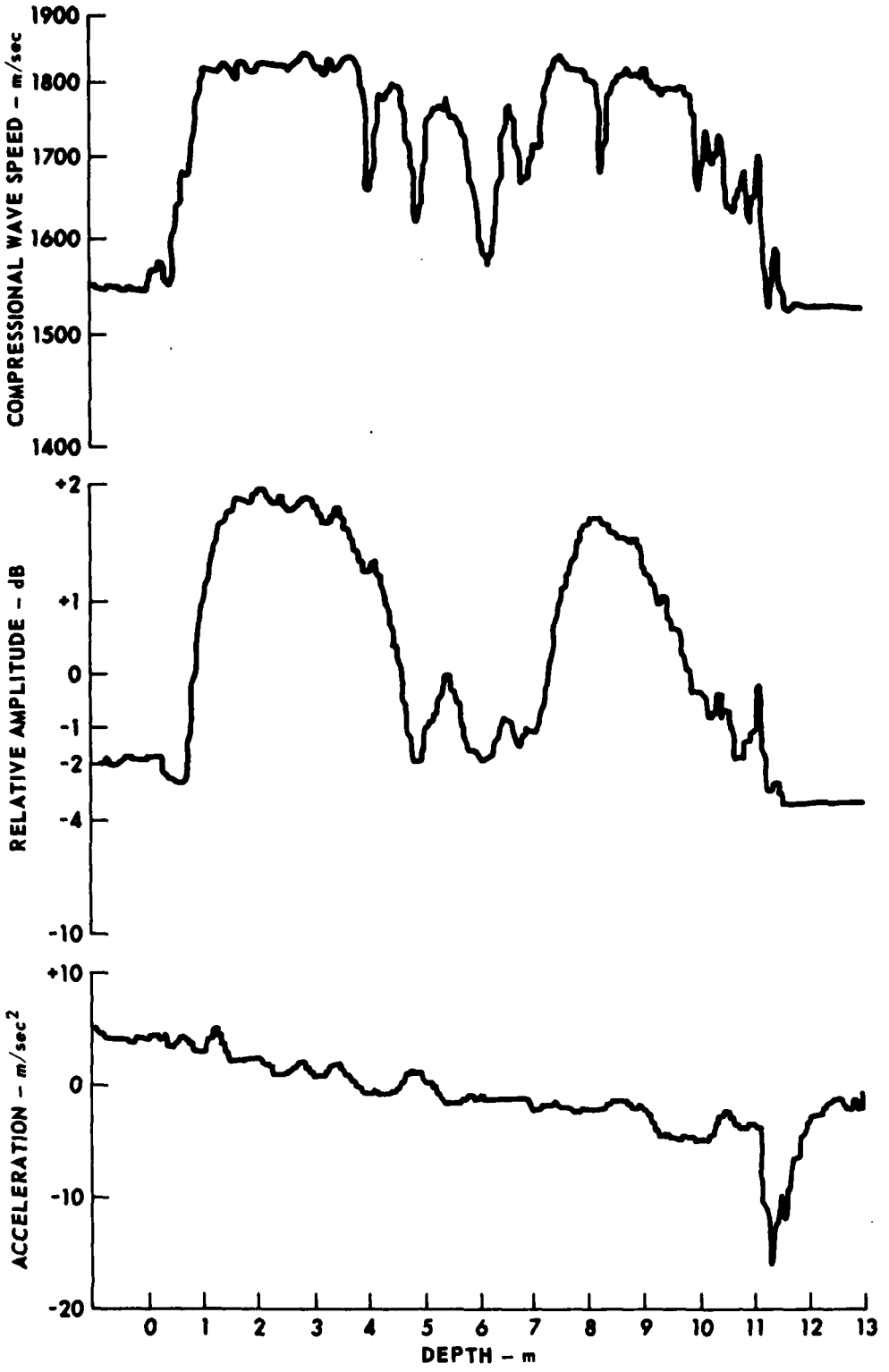

FIGURE 8
COMPRESSIONAL WAVE PROFILES FOR CORE 7
R/V GYRE

ARL:UT
AS-80-948
DJS-GA
3-21-80

The relative amplitude of the received pulses varies over a range of 4 dB and generally follows the shape of the speed curve. The reason for the increase in signal amplitude in the higher speed sediment over that in the water is that the higher acoustic impedance of the sediment matches the acoustic impedance of the transducer elements more closely and reduces the insertion loss of the sediment-transducer system. Zero on the relative amplitude scale is the amplitude measured at room temperature and atmospheric pressure during calibration. Changes in temperature and pressure cause the loss of amplitude in the bottom water.

III. LABORATORY MEASUREMENTS

A. Introduction

Development of appropriate compressional wave and shear wave techniques for in situ measurements has enabled development of an extensive laboratory measurements program to augment the in situ measurements. Examination of the links between acoustic propagation and measurable physical parameters is an important aspect of the program of acoustical measurement of sediment. In the past year, effort has been focused on developing theoretical models for compressional wave attenuation in various sediment types and on the examination of temperature influences on compressional wave and shear wave propagation in sediments.

All of the laboratory work for the past year has been submitted for journal publication;[10-12] the contents of each manuscript are contained in this section; figure numbers, equation numbers, and reference numbers have been changed to fit the body of this report.

B. Viscous Attenuation of Sound in Saturated Sand

INTRODUCTION. In underwater acoustics there is need for accurate values of the attenuation of sound in marine sediments. In particular there is a need for attenuation values at low enough frequencies to be of interest to long range sonar propagation. However, in practice direct measurements of attenuation at low frequencies are difficult to obtain; often the low frequency values must be extrapolated from measurements obtained at higher frequencies. Consequently, to extrapolate to lower frequencies there is a need for accurate description of and theoretical models for loss mechanisms of sound propagation in marine sediments.

The most comprehensive theory of wave propagation in saturated porous media is that formulated by Biot.[20-22] This theory embodies many of the earlier theories as special cases; the significant new feature is that it allows for the movement of the fluid relative to the solid frame and thus for the possibility of a viscous fluid loss. This loss will increase with frequency (f) proportional to f^2 for lower frequencies and proportional to $f^{1/2}$ at higher frequencies. Practical application of Biot's theory was rather limited until Stoll and Bryan[23] in 1969 and later Stoll[24,25] applied the theory to attenuation as a function of frequency in marine sediments. They included loss terms for the elastic parameters of the solid frame and thereby took into account losses due to grain-to-grain contact as well as the aforementioned fluid loss. They pointed out that fluid losses may represent a significant factor in high frequency attenuation in sand and therefore that common linear extrapolation to lower frequencies may result in significant errors.

A major difficulty in the application of the Biot-Stoll theory is that the relative importance of the loss terms as well as the meaning of "high" and "low" frequencies depends on several parameters which are rather difficult to calculate in practice. The viscous loss will in particular depend on permeability, pore size, and the mass coupling between the solid and fluid. The mutual relationship between these parameters and their relationship to the form and size distribution of the grains as well as the porosity of the bulk material is in general difficult to describe and can probably only be obtained experimentally (if at all). From a practical point of view, however, this may not be important since only fluid loss is expected to be of potential importance for sound propagating in sands with rather uniform grains and high permeability. Therefore in the following we shall limit discussion to this case and show that all the important dynamic parameters can in fact be estimated from a knowledge of grain size and porosity. Predicted values for the viscous loss will then be compared with some new measurements on saturated glass beads and with earlier measurements in sand.

THEORETICAL CONSIDERATIONS. In his original paper Biot[21] first considered laminar flow in a circular tube and generalized the result to tubes of other cross-sections. In the following we shall briefly review that part of the treatment which is important to the present discussion.

Considering laminar flow of a viscous fluid in a circular tube of radius a, Biot showed that the frictional stress τ caused by the shearing wave in the fluid is

$$\tau = \frac{4}{a} \eta F(\kappa)(u_1 - u_2) \quad , \tag{1}$$

where u_1 is the velocity of the tube and u_2 is the mean velocity of the fluid which has viscosity η. $F(\kappa)$ is a function of (angular) frequency ω, which accounts for the deviation from Poiseuille flow at higher frequencies given by

$$F(\kappa) = \frac{1}{4} \frac{\kappa T(\kappa)}{1 - \frac{2i}{\kappa} T(\kappa)} \quad , \tag{2}$$

where $T(\kappa)$ is given by the complex Kelvin function

$$T(\kappa) = \frac{\mathrm{ber}'(\kappa) + \mathrm{bei}'(\kappa)}{\mathrm{ber}(\kappa) + \mathrm{bei}(\kappa)} \quad , \tag{3}$$

and the argument κ is

$$\kappa = a(\omega \rho_f / \eta)^{1/2} \quad . \tag{4}$$

Introducing the Darcy coefficient of permeability B_o, which for a circular duct is $B_o = a^2/8$, the frictional force per unit volume can be written

$$z = \frac{\eta}{B_o} \frac{a}{2} F(\kappa) \quad , \tag{5}$$

and the equations of motion for harmonic excitation are expressed by

$$Q_1 = i\omega \rho_1 u_1 + z(u_1 - u_2) \frac{2}{a}$$

and (6)

$$Q_2 = i\omega \rho_2 u_2 - z(u_1 - u_2) \frac{2}{a} \quad ,$$

where Q_1 and Q_2 can be interpreted as volume forces acting, respectively, on the tube and the fluid which have masses per unit volume of ρ_1 and ρ_2. Since $F(\kappa)$ is a complex function with real part $F_r(\kappa)$ and imaginary part $F_i(\kappa)$, these equations can be written in the form

$$Q_1 = i\omega\left[\rho_1 + \frac{\eta}{B_o}\frac{F_i(\kappa)}{\omega}\right]u_1 - i\omega\frac{\eta}{B_o}\frac{F_i(\kappa)}{\omega}u_2 + \frac{\eta}{B_o}F_r(\kappa)(u_1-u_2) \quad ,$$

and (7)

$$Q_2 = -i\omega\frac{\eta}{B_o}\frac{F_i(\kappa)}{\omega}u_1 + i\omega\left[\rho_2 + \frac{\eta}{B_o}\frac{F_i(\kappa)}{\omega}\right]u_2 - \frac{\eta}{B_o}F_r(\kappa)(u_1-u_2) \quad .$$

Comparison with Biot's original equations shows that the apparent mass $(-\rho_{12})$ of the fluid which is attached to the tube is given by the imaginary part of $F(\kappa)$ and is equal to

$$(-\rho_{12}) = \frac{\eta}{B_o}\frac{F_i(\kappa)}{\omega} \quad , \tag{8}$$

whereas the real part gives the frequency dependent flow resistance

$$R \simeq \frac{\eta}{B_o}F_r(\kappa) \quad . \tag{9}$$

In the low frequency limit $F(\kappa)\simeq 1+i\kappa^2/24$ and $R_o=\eta/B_o$, i.e., the static flow resistance. The apparent mass becomes $(-\rho_{12})_o=a^2\rho_f/(24B_o)$ which for a circular cross section reduces to $(-\rho_{12})_o=\rho_f/3$. In the high frequency limit $F(\kappa)\simeq\kappa(1+i)/4\sqrt{2}$ and

$$(-\rho_{12})_\infty \simeq \frac{a}{4B_o}\sqrt{\frac{\rho_f\eta}{2\omega}} = \frac{2}{a}\sqrt{\frac{\rho_f\eta}{2\omega}} \quad . \tag{10}$$

PERMEABILITY AND PORE SIZE PARAMETER. In the actual case of propagation in a porous medium the radius a must be replaced by a pore size parameter a_p and the permeability B_o should preferably be related to the texture of the medium. Returning to Eq. (5), the factor a/2 represents the surface of a unit length of the tube divided by the volume. This is commonly known as the hydraulic radius m defined by[26]

$$m = \frac{\text{volume filled with fluid}}{\text{wetted surface}} \quad . \tag{11}$$

For a medium composed of uniform spherical grains of diameter d_m and porosity ϕ it can be shown that

$$m = \frac{\phi}{1 - \phi} \frac{d_m}{6} \quad . \tag{11}$$

Since Biot showed that the actual form of the function $F(\kappa)$ is not very dependent on the shape of the pores, we therefore propose to retain the frequency correction of Eq. (2) with the radius replaced by a pore size parameter a_p given by

$$a_p = 2m = \frac{d_m}{3} \frac{\phi}{1 - \phi} \quad . \tag{12}$$

The specific permeability of a porous medium is based on Darcy's law, which states that the rate of flow is proportional to the pressure gradient and inversely proportional to the viscosity. This implies that the flow resistance is entirely due to viscous drag and that no other chemical or electrical effects are important. Although the permeability often can only be determined experimentally, it is also true that for media composed of regular grains the permeability can be approximately calculated from the Kozeny-Carman equation, which is[26]

$$B_o = \frac{\phi m^2}{k} \quad ,$$

where m is the earlier defined hydraulic radius. With spherical grains this gives

$$B_o = \frac{d_m^2}{36k} \frac{\phi^3}{(1-\phi)^2} \quad . \tag{14}$$

The coefficient k takes into account the pore shape and the tortuosity of the pores. For circular tubes k=2, whereas for spherical grains both theoretical considerations and experiment seem to confirm that k≈5. This value and Eq. (14) have been checked by Bell,[14] who plotted measured values of B_o as a function of ϕm^2 (Fig. 9). The values for the glass beads of different sizes, the Ottawa sand (OTT), and the Panama City sand (PC) are new data and the other sand data are taken from an earlier investigation by Mifsud,[27] later reported by Nolle et al.[28] As can be seen from Fig. 9 the measured values are reasonably close to a straight line with a slope corresponding to k≈5.

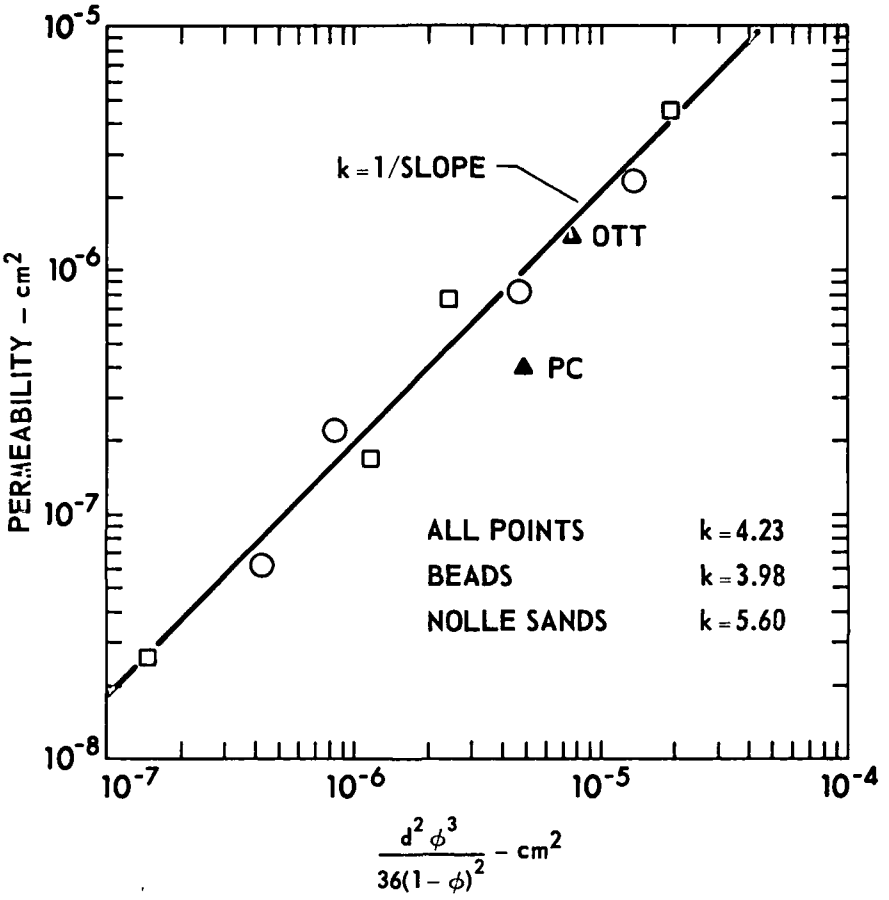

FIGURE 9
SEDIMENT PERMEABILITY AS A FUNCTION OF GRAIN SIZE AND POROSITY

ARL:UT
AS-79-207-P
JMH - GA
2 - 7 - 79
REV 3-21-79

STRUCTURE CONSTANT. Introducing the dilatation e of the bulk material and the relative dilatation ζ of the fluid, the coupled differential equations which govern the wave propagation can be written in the form[29]

$$\nabla^2(He-C\zeta) = \partial^2/\partial t^2(\rho e-\rho_f\zeta) \quad , \tag{15a}$$

$$\nabla^2(Ce-M\zeta) = \partial^2/\partial t^2(\rho_f e-\rho_c\zeta) - (\eta/B_o)F_r(\kappa)\partial\zeta/\partial t \quad . \tag{15b}$$

The coefficients H, C, and M are elastic coefficients given by the bulk modulus of the mineral grains K_r, the shear and bulk moduli of the free draining frame μ_b and K_b, and the porosity ϕ.[23,30]

$$H = K + \frac{4}{3}\mu_b \quad , \tag{16}$$

with

$$K = K_r(K_b+Q)/(K_r+Q) \quad , \tag{17}$$

$$Q = (K_f/\phi)(K_r-K_b)/(K_r-K_f) \quad , \tag{18}$$

$$C = QK_r/(K_r+Q) \quad , \tag{19}$$

and

$$M = CK_r/(K_r-K_b) \quad . \tag{20}$$

The densities of the fluid and the solid are ρ_f and ρ_s and the density of the aggregate is $\rho=(1-\phi)\rho_s+\phi\rho_f$. Equation (15) is of the same form as used by Stoll except that only the real part of $F(\kappa)$ is used in the last part of Eq. (15b), which therefore becomes a true loss term, and ρ_c then becomes

$$\rho_c = \frac{\rho_f}{\phi} + \frac{\eta}{B_o}\frac{F_i(\kappa)}{\omega}$$

$$= \frac{\rho_f}{\phi}\left(1 + \frac{\eta\phi}{B_o\rho_f}\frac{F_i(\kappa)}{\omega}\right) \quad . \tag{21}$$

Because part of the fluid is attached to the skeleton frame ρ_c is larger than ρ_f/ϕ with a factor γ which is given by

$$\gamma = 1 + \frac{\eta\phi}{B_o\rho_f} \frac{F_i(\kappa)}{\omega} \quad . \tag{22}$$

Stoll calls this factor a structure constant and states that it can only be determined experimentally. However, the preceding discussion shows that the factor is frequency dependent and can be calculated, at least for aggregates with a permeability which follows Eq. (14). Using Eqs. (12) and (14) together with the limiting values of $F(\kappa)$, it is easy to show that in the low frequency limit γ becomes

$$\gamma_o \simeq 1 + \frac{k}{6} \quad . \tag{23}$$

For a medium composed of circular tubes, k=2 giving γ_o=4/3 in agreement with the discussion following Eq. (9). For spherical grains with k=5, we obtain γ=1.8, a value which is not very different from the value used by Stoll and which is also close to the values indicated by the experiment performed by Domenico.[31] Figure 10 shows a plot of γ as a function of frequency calculated for a medium grain diameter $d_m = 1.65 \times 10^{-2}$ cm, porosity ϕ=0.37, and a permeability in agreement with Eq. (12). The structure constant remains fairly stable up to a frequency

$$\omega \simeq \frac{64\eta}{a^2\rho_f} \quad . \tag{24}$$

In principle the same approach can be used to find the structure constant for media with irregular grains of different sizes and lower permeability. In this case the k will be higher, the porosity will be lower, and the structure constant will remain high up to quite high frequencies. The effect of nonconnected pores can, in principle, be taken into account by using a correspondingly reduced porosity when calculating the pore size parameter (Eq. 12).

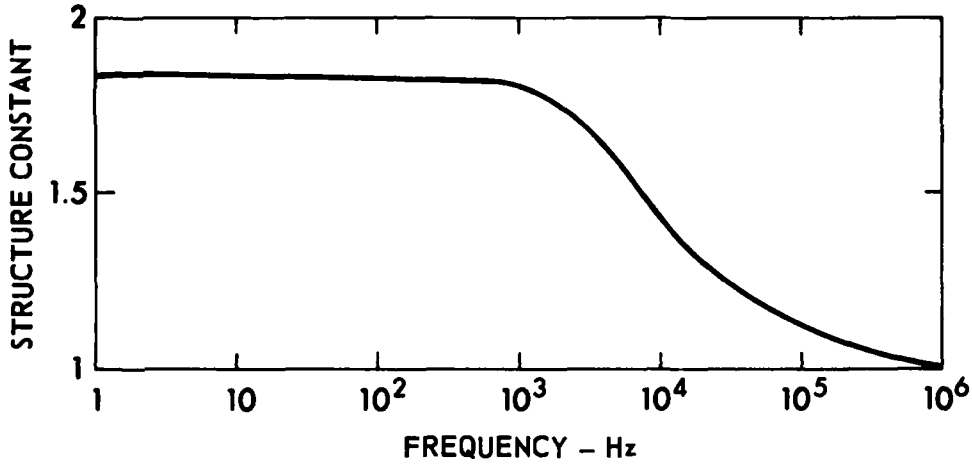

FIGURE 10
STRUCTURE CONSTANT AS A FUNCTION OF FREQUENCY
CALCULATED FOR A SEDIMENT WITH SPHERICAL GRAINS

GRAIN SIZE = 1.65×10^{-2} cm
POROSITY = 0.37

ARL:UT
AS-79-438-P
JMH-GA
3-21-79

VISCOUS ATTENUATION AND VELOCITY DISPERSION. Assuming harmonic waves, Eq. (15) can easily be converted to a frequency equation of fourth degree, from which we can find both the velocity and attenuation of the compressional waves of the first and second type. In practice this calculation is most conveniently done on a computer and this has been done for the numerical examples in the next section. To see the importance of the different terms it is, however, instructive to obtain approximate expressions valid at high and low frequencies, and this will be done in the following.

In many cases $C^2 \simeq HM$ and then the frequency equation reduces to a second order equation. In the low and high frequency limit, we can then find the following approximate expressions for the low and high frequency viscous attenuation,

$$\alpha_o = \frac{\Delta v}{v_o^2} \frac{1-\phi}{\phi} \frac{\rho_s}{\rho} B_o \frac{\omega^2 \rho_f}{\eta} \quad , \tag{25}$$

$$\alpha_\infty = \frac{1}{4\sqrt{2}} \frac{\Delta v}{v_\infty^2} \frac{\phi}{1-\phi} \frac{\rho}{\rho_s} \frac{a_p}{B_o} \left(\frac{\omega \eta}{\rho_f}\right)^{1/2} \quad . \tag{26}$$

With v_o and v_∞ being the sound velocities at low and high frequencies, $\Delta v = v_\infty - v_o$ is the total velocity dispersion. As can be seen the attenuation is proportional to B_o at low frequencies and to $B_o^{-1/2}$ at high frequencies, as follows from Eqs. (12) and (13). In the low frequency limit the sound velocity will approach the "closed system" velocity,

$$v_o = (H/\rho)^{1/2} \quad . \tag{27}$$

For very high frequencies the velocity will be higher mainly because the fluid mass is decoupled from the frame, and the velocity will be approximately

$$v_\infty = \left(\frac{H}{\rho_s(1-\phi)}\right)^{1/2} \quad . \tag{28}$$

EXPERIMENTAL RESULTS. In this section the theory will be compared with some new measurements of sound velocity and attenuation in saturated glass beads and some earlier reported measurements in sands. The permeability, porosity, and grain size distribution as well as the elastic parameters of the solid and fluid are known in all of the considered cases. The only parameter which is not known is the bulk and shear modulus of the frame. In principle these parameters can be determined by measuring compressional and shear wave velocities in the dry media but such measurements have proved to be difficult or inaccurate without a heavy overburden pressure.[31] The problem was solved by choosing $u_b = K_b$, corresponding to a Poisson's ratio of 0.125, and adjusting K_b until the observed and calculated velocities were in agreement for one particular frequency in the observed interval. The same method is used by Hamilton,[30] but since he is using the "closed system" velocity v_o [Eq. (27)], his values for K_b will always be higher than ours. We find, for instance, $K_b \simeq 10^9$ dyn/cm^2 in sand as compared with Hamilton's $K_f \simeq 10^{10}$ dyn/cm^2. For glass beads we found $K_b = 6 \times 10^9$.

MEASUREMENTS ON GLASS BEADS. Sound velocity and attenuation have been measured for water saturated glass beads of mean diameter $d_m = 1.8 \times 10^{-2}$ cm at a temperature of about 20°C. The "grain" density of the glass beads was 2.5 g/cm^3 and the saturated bulk density was 1.92 at a porosity of 0.365 ±0.008. The measurements were performed in a tank 45 cm deep x 70 cm long x 50 cm wide. A spherical 2.54 cm (1 in.) diam ceramic transducer was used as a projector and the receiver was a 1.25 cm (0.5 in.) diam ceramic disc. The depth of the transducers was about 20 cm and the distance between transmitter and receiver varied from 10 to 22 cm. The maximum frequency was about 300 kHz, limited by noise, and the lowest frequencies were about 10 to 20 kHz, limited by interference. Before the measurements the beads were washed and boiled to remove air and during the measurements the tank was vibrated after every change in receiver and/or transmitter position.

For each frequency the signal amplitude and arrival time were measured at from four to five transmitter/receiver separations using

an oscilloscope with a digital readout of the time delay. The measurements were done on one of the leading peaks of the received signal. Attenuation and velocity values were obtained after regression analysis of the data as a function of separation. This showed quite consistent results in the upper frequency region but more variability in the lower frequency region, in particular for the attenuation value (see Table I); this is to be expected since the total attenuation over the path length is very small for the lowest frequencies.

The same experiment was also performed in water showing that the geometrical spreading was very close to spherical and giving a sound velocity of 1490 m/sec with a variation within 0.5 m/sec over the whole frequency range. This value is, however, approximately 10 m/sec higher than values predicted from the normal empirical equations for the sound speed in fresh water. If anything, this may indicate that the experimental method and analysis give a small but insignificant bias to the velocity results.

Figure 11 shows the measured and theoretical values of the sound velocity as a function of frequency for the saturated beads. As already explained, the theoretical curve is obtained after adjusting the elastic parameters of the frame so that the theoretical value agrees with the experimental value for one particular frequency (100 kHz). The importance of the theoretical curve is therefore not the absolute velocity but rather the velocity dispersion which is predicted by the theory. As can be seen from Fig. 11 the experimental values give a clear indication of dispersion and the agreement with theory is quite good. The dispersion is, however, very small and difficult to detect unless the measurements cover a wide band in the most sensitive frequency region.

Figure 12 shows the measured attenuation together with the theoretical curve for viscous attenuation. The latter was calculated from the model using the same elastic parameters for the frame as those that gave the best fit to the velocity data. Again the general agreement is quite good but there is considerable scatter in the data and the theoretical values appear to be somewhat higher than the experimental results, for the lower frequencies in particular.

TABLE I

TABLE OF MEASUREMENTS IN SATURATED

GLASS BEADS

FREQUENCY kHz	VELOCITY m/sec	ATTENUATION dB/m
15	1887.86	-----
20	1897.37	2.80
30	1906.41	3.60
40	1915.95	6.98
50	1919.95	11.18
60	1918.05	24.86
80	1919.26	17.63
100	1922.33	13.20
150	1926.78	19.65
200	1942.38	26.46
300	1928.99	33.79

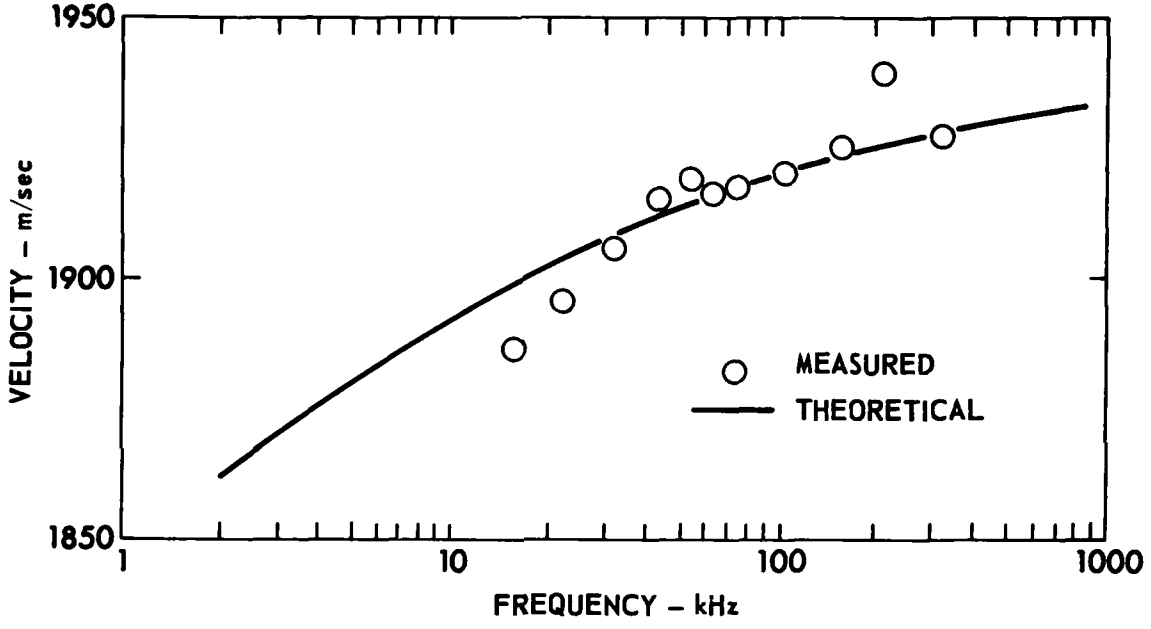

FIGURE 11
COMPRESSIONAL WAVE VELOCITY AS A FUNCTION OF FREQUENCY FOR WATER SATURATED GLASS BEADS
POROSITY = 0.365

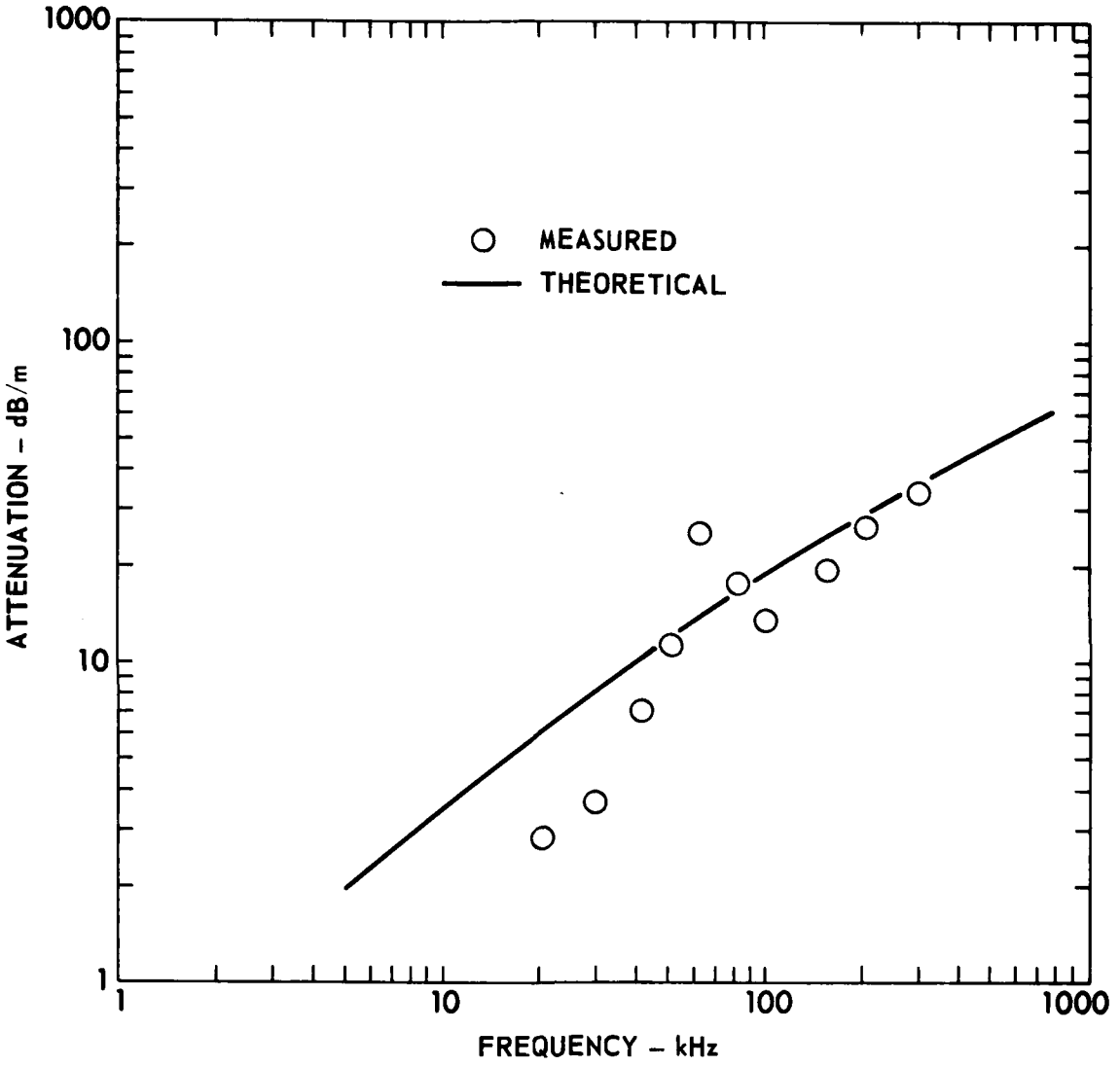

FIGURE 12
COMPRESSIONAL WAVE ATTENUATION AS A FUNCTION OF FREQUENCY FOR WATER SATURATED GLASS BEADS
POROSITY = 0.365

ARL:UT
AS-79-440-P
JMH - GA
3 - 21 - 79

MEASUREMENTS IN SAND. In this section some earlier measurements of attenuation in water saturated sand will be compared with theoretical calculations of viscous attenuation. This discussion will be limited to sand for which the permeability either is known from measurements or can with confidence be estimated from Eq. (14).

Attenuation in four different graded sands and for frequencies from 0.2 MHz to 1 MHz has been measured by Mitsud[27] and later reported by Nolle et al.[28] They found, in agreement with Eq. (25), the attenuation to be inversely proportional to the grain size and to increase with $f^{1/2}$. For this reason they do not give the individual measurements but an average coefficient with which the attenuation can be calculated.[32] At a later time Hampton[33] measured the attenuation in three of the same sands in the frequency range of 10-30 kHz. Figure 13 shows the two groups of experimental results together with the calculated viscous attenuation. The theory agrees reasonably well with the results for both groups and in particular agrees very well with their slope, which is close to f for the 3ϕ sand at 10 kHz and $f^{1/2}$ at the high frequency limit.

Hamilton[34] has compiled many measurements of attenuation in sediments. We have taken his values for all grades of sand and compared them with the calculated viscous attenuation for fine (3ϕ) and coarse (0.7ϕ) sand. As can be seen from Fig. 14 the experimental values are quite close to the theoretical values suggesting that viscous losses may be important for high frequencies in sand.

CONCLUSION. Based on Biot's theory for the propagation of sound in a fluid saturated porous media and also Stoll's earlier work, the viscous attenuation of sound has been studied both theoretically and experimentally.

A relationship is found between the size of the pores and the permeability of the medium from which the mass coupling effect between fluid and rigid frame can be calculated as a function of frequency.

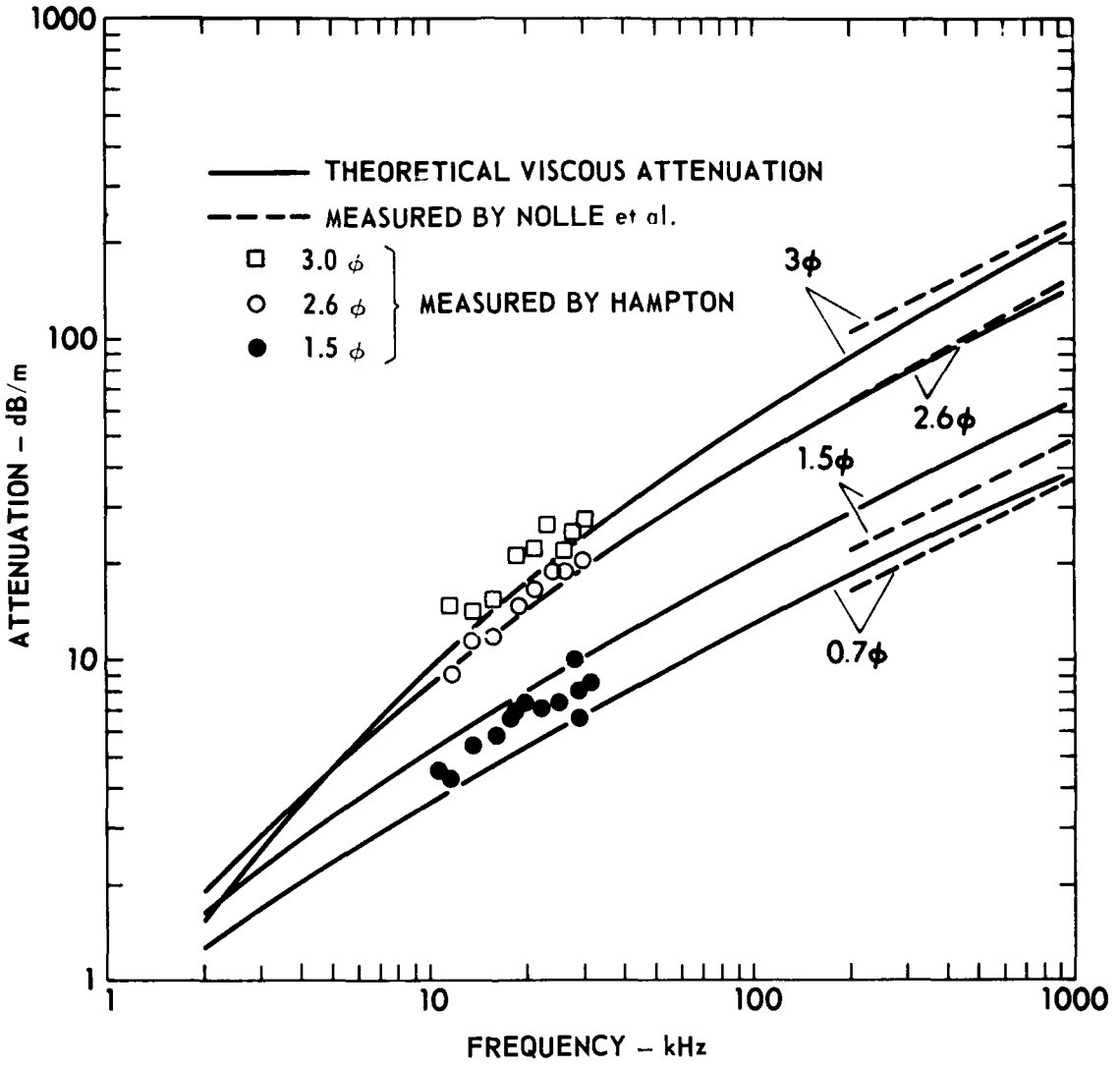

FIGURE 13
COMPRESSIONAL WAVE ATTENUATION AS A FUNCTION
OF FREQUENCY FOR WATER SATURATED SANDS

ARL:UT
AS-79-441-P
JMH - GA
3 - 21 - 79

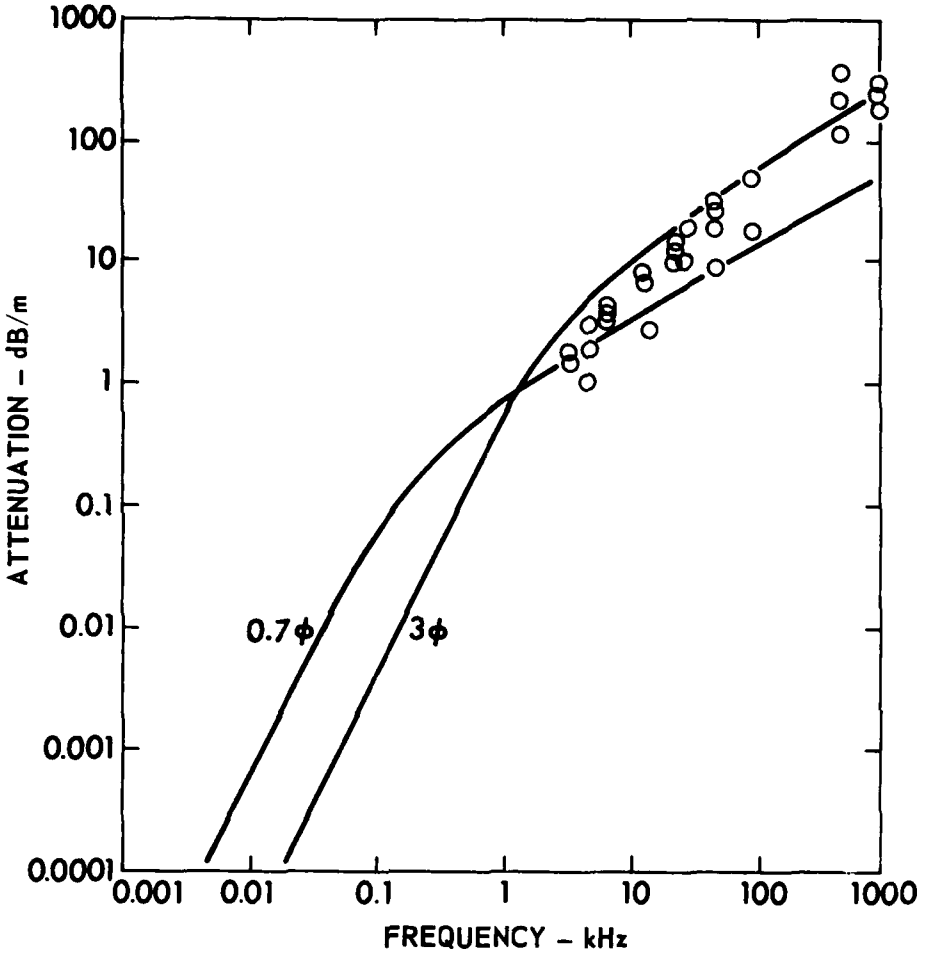

○ MEASUREMENTS IN SANDS OF ALL SIZES, COMPILED BY HAMILTON (1972).

—— THEORETICAL VISCOUS ATTENUATION FOR SAND OF GRADE 0.7 ϕ AND 3.0 ϕ.

FIGURE 14
COMPRESSIONAL WAVE ATTENUATION AS A FUNCTION OF FREQUENCY FOR WATER SATURATED SANDS

ARL:UT
AS-79-442-P
JMH - GA
3-21-79

Measurements of attenuation and sound velocity in water saturated glass beads in the frequency range 20-300 kHz are in good agreement with theory. The small velocity dispersion predicted by the theory seems to be confirmed experimentally.

Earlier measurements of attenuation in sand compare with theoretical viscous attenuation; this indicates that viscous attenuation may be of significant importance in sand at relatively high frequencies.

Viscous attenuation will increase with f^2 at low frequencies and with $f^{1/2}$ at high frequencies. However, in the intermediate frequency region where most attenuation measurements are done, both in situ and in the laboratory, the increase is not very different from f^1. Consequently, experimental evidence that attenuation increases linearly with frequency does not rule out the possibility that viscous attenuation may be important.

This study has concentrated on viscous attenuation in sand of high permeability and at relatively high frequencies. For lower frequencies and in media with less permeability the viscous losses will be much smaller and other forms of losses are likely to be of dominating importance.

C. Viscous Attenuation of Sound in Suspensions and High Porosity Marine Sediments

INTRODUCTION. In the preceding section Biot's theory[20,21] for sound propagation in porous media and also the results of Stoll's work[23-25] were applied to determine the viscous attenuation of sound in saturated sand.[10] A comparison between theory and experiment indicates that viscous attenuation may predominate in sands of high permeability having uniform and regular grains.

In the Biot model the most important parameters for viscous attenuation are permeability and pore size. For sand these can be estimated with some confidence and the permeability can also be measured quite accurately. For silt and clay the situation is different; the permeability as known from

soil mechanics is often extremely low, and large distributions in grain size and shape make it very difficult to assign values to the pore size parameters.

Another model applied to high porosity silt and clay is the suspension model derived by Urick[35] and Urick and Ament.[36] One advantage of this model is that it can be applied to cases where the grains are distributed in size; on the other hand, it is known to fail when the concentration exceeds a few percent.

Since we therefore have two models which may be applied to calculate viscous attenuation in high porosity marine sediments, it is interesting to compare predictions from them and also to compare these results with available experimental data. In the following we will briefly review the two models, derive simplified expressions for sound velocity and attenuation as a function of frequency, and discuss the limitations which follow from these assumptions.

To compare Biot's theory with the suspension theory we will have to assume that the medium has no frame rigidity, i.e., that both the shear modulus and the frame bulk modulus are zero. This results in a reduced Biot model where the only loss mechanism considered is the viscous loss due to relative motion between the frame and the fluid.

Both models assume that the medium is composed of spherical particles dispersed in a viscous fluid and that there are no other mechanical, electrical, or chemical forces interacting with the particles. Compared with the properties of real sediments as discussed by Hamilton,[30] this represents a strong simplification which can only be valid for high porosity sediments, if at all.

THE MODELS

The Biot Model. In general, the Biot model describes the wave propagation by two coupled differential equations giving as the solution two dilational waves. When both the shear and the bulk moduli of the frame are zero the

solutions reduce to one wave with a complex wave number which can be expressed by

$$(\ell/w)^2 = \frac{K}{\rho} \frac{\left(\frac{1-\phi}{\phi}\right)(\rho_s\rho_f/\rho) - i\eta[F(\kappa)/\omega B]}{\left(\frac{1-\phi}{\phi}\right)\rho^* - i\eta[F(\kappa)/\omega B]} \quad . \tag{29}$$

Here K is the system bulk modulus given by

$$K^{-1} = \phi K_f^{-1} + (1-\phi)K_s^{-1} \quad , \tag{30}$$

where K_f and K_s are the bulk moduli of the fluid and solid, respectively, and ϕ is the porosity. The density of the aggregate is ρ and ρ^* is a fictional density given by

$$\rho^* = (1-\phi)\rho_s + \phi\rho_f \quad , \tag{31}$$

with ρ_f being the fluid density and ρ_s the solid density. The fluid viscosity is η and B is the absolute permeability of the medium. The function $F(\kappa)$ is a function of (angular) frequency which accounts for the deviation from Poiseuille flow at higher frequencies. $F(\kappa)$ is normally determined[21] by assuming that the fluid flows in circular tubes or pores of radius a_p and then the argument is given by

$$\kappa = a_p(\omega\rho_f/\eta)^{1/2} \quad , \tag{32}$$

and $F(\kappa)$ is given by complex Kelvin functions.

As stated before, a major problem with the Biot model is to find reasonable values for B and a_p. In the previous study[10] we used the Kozeny-Carman equation which gives B as

$$B = a^2/ak_o\ \phi^3/(1-\phi)^2 \quad , \tag{33}$$

where a is the radius of the grains, and we have proposed to use as the pore size parameter

$$a_p = a/\sigma\ \phi/(1-\phi) \quad . \tag{34}$$

The factor k_o in Eq. (33) is constant which takes into account the tortuosity and the shapes of the pores. The values and variability of k_o as functions of porosity and of shape and size distributions of the grains are discussed by Carman.[26] With spherical and uniform grains the value of k_o will be approximately 5; with elongated grains of different sizes the value of k_o will be somewhat higher, around 10. The value of k_o will also increase rapidly when the porosity becomes higher than about 95%.

The values given by Eq. (33) do not agree with values found in the literature for silt and clay. Reference is made here to Bryant et al.[37] who have collected permeability values for a wide range of marine sediments. The data display considerable scatter, but they conclude that the mean value of the absolute permeability is given by the void ratio e according to $B = 10^{-14} \times e^5$ cm^2. A void ratio of e=2, which corresponds to a porosity of 67%, thus gives $B \simeq 3 \times 10^{-3}$ cm^2. With the same porosity and a mean particle radius of $a = 7.8 \times 10^{-4}$ cm (6ϕ), Eq. (33) gives $B \simeq 10^{-8}$ cm^2. It will later be shown that at low frequencies Eq. 29 gives an attenuation which is proportional to B. Which of the two cited values is used will therefore have a very strong effect on the predicted value of viscous loss. However, it should be pointed out that permeability as evaluated by soil mechanics[37] serves an entirely different purpose than prediction of sound transmission. In fact, the permeability of soil mechanics is a static measure obtained by measuring unidirectional flow over an extended time, and it is not obvious that values obtained in this way can be applied to the very dynamic situation we are confronted with here.

THE SUSPENSION MODEL. A theoretical model for sound propagation in a suspension based on scattering theory was first formulated by Urick[35] and Urick and Ament.[36] When a plane wave of pressure amplitude p_o is incident on a spherical particle at the origin, the scattered wave p_s, at a location specified by the coordinator r and ϕ, is given by

$$\rho_s(\theta,r) = \rho_o \frac{e^{i\ell_f r}}{r} \phi(\theta) \quad , \tag{35}$$

where

$$\Phi(\theta) = \frac{1}{3}\, \ell_f^2 a(\gamma_o+\gamma_1\cos\theta) \quad , \tag{36}$$

with ℓ_f being the wave number of the fluid.

The monopole scattering is determined by

$$\gamma_o = \left(K_s^{-1}-K_f^{-1}\right)\Big/K_f^{-1} \quad . \tag{37}$$

The dipole scattering is given by γ_1, which depends on the density contrast of the fluid. The expression given by Urick and Ament[36] is, with some changes in notation,

$$\gamma_1 = \sigma A/(\sigma+A) \quad , \tag{38}$$

where

$$\sigma = (\rho_s-\rho_f)/\rho_f \quad , \tag{39}$$

and

$$A = \frac{3}{2}\left(1 + \frac{3}{2\beta a}\right) + i\,\frac{9}{4\beta a}\left(1 + \frac{1}{\beta a}\right) \quad . \tag{40}$$

Here $\beta=(\omega_f/2\eta)^{1/2}$ and β^{-1} is the characteristic thickness of the shear boundary layer in the fluid around the particle. It has been assumed that the particle is much smaller than the wavelength so that Rayleigh scattering can be ignored. Considering now the scattered waves from a number of randomly spaced particles, the sound propagation through the composite material is characterized by a complex wave number ℓ given by

$$(\ell/\omega)^2 = K_f/\rho_f\,[1+\delta\gamma_o][1+\delta\gamma_1] \quad , \tag{41}$$

where $\delta=1-\phi$ is the volume concentration of particles.

This result, but with viscosity neglected, was also obtained by Waterman and Truell[38] who, in addition, established a criterion for the validity of Eq. (41) with respect to multiple scattering. They found that Eq. (41) is correct in the weak scattering limit defined by the requirement that $(nQ_s/\ell_f)<<1$, where $n=\delta/(4\pi a^3/3)$ is the volume density

of the particle and Q_s is the scattering cross-section of a single particle given by

$$Q_s = \frac{4}{9}\pi a^2(\ell_f a)^4\left[\gamma_o^2 + \frac{1}{3}\left|\gamma_1\right|^2\right] \quad . \tag{42}$$

Since the value of $\gamma_o^2+1/3\left|\gamma_1\right|^2$ will be about unity for sediments, the weak scattering condition becomes $\delta<<3(\ell_f a)^3$, a condition which is satisfied for most cases and frequencies of practical interest.

A more important restriction involves the influence of viscosity on the dipole contribution γ_1. This value is calculated assuming that the fluid flow over a particle is not affected by the neighboring particles; it is an approximation which can only be true if the boundary layer thickness β^{-1} is much smaller than the distance between particles. Since the boundary layer thickness is inversely proportional to the square root of the frequency this condition will only be satisfied at high frequencies and low concentrations, but it is difficult to establish the exact region of validity.

COMPARISON AND DISCUSSION. In the following we will compare the two models and also make some comparisons with earlier measured values for sound velocity and attenuation in suspensions and sediments. To facilitate the comparison of the models and also to gain further insight into the effect(s) of the approximations involved, we will develop simplified expressions for velocity and attenuation that are valid at extremely low and extremely high frequencies, roughly defined $\beta a<<1$ and $\beta a>>1$, respectively. However, these expressions are used only as a basis for the discussion; the numerical examples are calculated by using the complete equations [Eqs. (29) and (41)]. The values of the fixed parameters used in the calculations are found in Table II.

SOUND VELOCITY. In the low frequency limit both models give the same expression for the sound velocity, known as Wood's equation,

$$N_o = (K/\rho)^{1/2} \quad , \tag{43}$$

TABLE II

VALUES OF THE FIXED PARAMETERS USED

IN THE MODEL CALCULATIONS

Parameter	Value
Fluid density	$\rho_f = 1$ g/cm^3
Solid density	$\rho_s = 2.65$ g/cm^3
Bulk modulus of fluid	$K_f = 2.15 \times 10^{10}$ dyn/cm^2
Bulk modulus of solid	$K_s = 3.6 \times 10^{11}$ dyn/cm^2
Fluid viscosity	$\eta = 10^{-2}$ dyn sec/cm^2

where K and ρ are given by Eq. (30) and Eq. (31), respectively. At high frequencies both models predict an increased velocity caused by the decrease in the effective density due to relative fluid-solid movement. The limiting velocities for the two models can be expressed in the following forms.

$$\text{Biot:} \qquad N_\infty^2 = v_o^2 \frac{\rho\rho^*}{\rho_f \rho_s} \quad , \tag{44}$$

$$\text{Susp:} \qquad N_\infty^2 = v_o^2 \frac{(\sigma+3/2)(1+\delta\sigma)}{\sigma + 3(1+\delta\sigma)/2} \quad . \tag{45}$$

Figure 15 shows the calculated velocities as a function of frequency. The grain size $a = 7.8 \times 10^{-4}$ cm (6ϕ), the porosity is 65%, and for the Biot model a_p and B are calculated using Eq. (34) and Eq. (33), respectively, with k_o=10. Also shown in Fig. 15 are Hampton's[33] measured values for "black sediment", which has almost the same mean grain size and porosity as for the calculated values. The theories give slightly higher velocities than those measured, but this could easily be corrected by minor changes in the assumed parameter values. The measured dispersion appears to agree well with the theory.

ATTENUATION. At low frequencies the limiting expressions for the viscous attenuation can be expressed as

$$\text{Biot:} \qquad \alpha_o = \frac{(1-\phi)^2}{2} \frac{(\rho_s-\rho_f)^2}{\rho v_o} \frac{B\omega^2}{\eta} \quad , \tag{46}$$

$$\text{Susp:} \qquad \alpha_o = \frac{(1-\phi)}{9} \frac{(\rho_s-\rho_f)^2}{\rho v_o} \frac{a^2\omega^2}{\eta} \quad . \tag{47}$$

The two expressions are very similar, having the same dependence on frequency and on density ratio. The difference between the two expressions is in the relationship between particle size, porosity, and permeability.

At low frequencies the suspension model gives the same attenuation as the Biot model if the latter uses a permeability given by

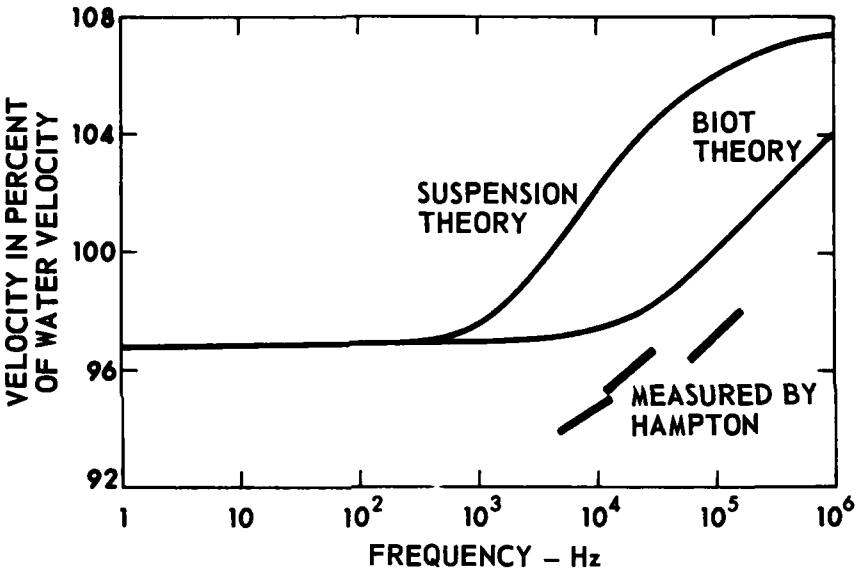

FIGURE 15
COMPRESSIONAL WAVE VELOCITY AS A FUNCTION OF FREQUENCY FOR A WATER SATURATED CLAY

ARL:UT
AS-79-2003-P
JMH - GA
9 - 25 - 79

$$B = \frac{2}{9} \frac{a^2}{1 - \phi} \quad . \tag{48}$$

This is an interesting result since it can also be derived directly from Stokes law for the resistance to fluid flow caused by a spherical particle of radius a. In a fluid flow of unit velocity this resistance is given by $D=6\pi\eta a$. With a volume concentration of n particles, $n=(1-\phi)/(4\pi a^3/3)$, the total resistance becomes $D=6\pi\eta a(1-\phi)/(4\pi a^3/3)$, which directly gives the permeability of Eq. (48). This assumes, however, that the flow around a single particle is completely unaffected by the presence of the other particles, which can be true only when the concentration of particles is extremely low. One should expect that when the concentration increases above a few percent the flow resistance will increase significantly, thereby reducing the attenuation compared with the linear increase with concentration as predicted by the suspension theory. The mutual effect of a higher concentration of particles on the fluid flow is on the other hand taken into account in the Kozeny-Carman equation. When it is used in the Biot model one should expect to get approximately correct low frequency attenuation values for concentrations higher than a few percent.

With B from Eq. (33) we see that at low frequencies the suspension model will give an attenuation which is higher than the Biot model by a factor of m, given by

$$m = 2k_o(1-\phi)/\phi^3 = 2k_o\,\delta/(1-\delta)^3 \quad . \tag{49}$$

This relationship will later be used to modify the suspension model.

In the extreme high frequency region the expressions for the attenuation become rather complicated but can be cast in the following forms.

Biot:
$$\alpha_\infty = \frac{a}{8\sqrt{2}} \frac{N_\infty^2 - v_o^2}{N_\infty^3} \frac{\phi}{1 - \phi} \frac{\rho}{\rho_s} \frac{a\rho}{B} \sqrt{\frac{\omega\eta}{\rho_f}} \quad . \tag{50}$$

$$\text{Susp:} \qquad \alpha_\infty = \frac{a}{\sqrt{2}} \frac{N_\infty^2 - v_o^2}{N_\infty v_o^2} \frac{\rho_f}{\rho_f + 2\rho_s} \frac{1}{a} \sqrt{\frac{\omega\eta}{\rho}} \quad . \tag{51}$$

Both models give attenuation proportional to $\omega^{0.5}$ at high frequencies and inversely proportional to the grain size. The actual values will depend on the values of a_p and B, but normally the Biot attenuation will be somewhat higher than the suspension model since the implied permeability in the suspension model is higher than that given by the Kozeny-Carman equation.

Figures 16 and 17 compare the attenuation predicted by Urick[39] and by Hampton[33] for kaolinite as a function of concentration. In Fig. 16 the mean particle diameter is 1μ and the frequency is 1 MHz. In Fig. 17 the mean particle diameter is 2μ and the frequency is 100 kHz. Both measurements are therefore in the low frequency region since $\beta a<1$. In the Biot model we have used Eq. (33) and Eq. (34) with the value $k_o=10$. As can be seen from the figures, and in agreement with both Urick's and Hampton's comments, the suspension models give much too high attenuation values for concentrations above a few percent. (McCann[40] has proposed a modification to the suspension model which, by taking into account interparticle forces, can be made to fit the measurements.) The Biot model on the other hand is in good agreement with the measurements, and in addition (although it cannot be seen from Figs. 16 and 17) gives the pleasingly correct result of zero viscous attenuation at 100% concentration.

VISCOUS ATTENUATION DEPENDENCY ON FREQUENCY. As can be seen from Eqs. (44), (50), and (51), the viscous attenuation will be proportional to ω^2 at low frequencies and to $\omega^{1/2}$ at higher frequencies. Since most measurements of attenuation as a function of frequency indicate a linear dependence on frequency,[34] this could indicate that viscous attenuation is much lower than the models predict and that other loss mechanisms are by far more important. The relative importance of the various loss mechanisms is a difficult issue and we do not have enough knowledge to resolve it now. We would, however, like to point out that in practical applications the viscous loss models also may give a viscous attenuation that increases

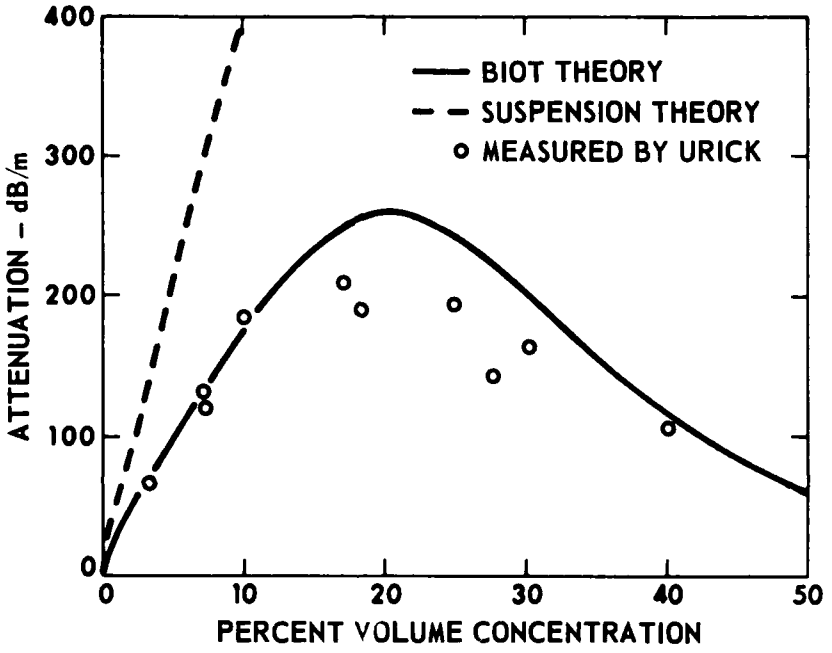

FIGURE 16
COMPRESSIONAL WAVE ATTENUATION AS A FUNCTION OF PARTICLE CONCENTRATION IN KAOLINITE CLAY
PARTICLE DIAMETER = 1 μ
FREQUENCY = 1 MHz

ARL:UT
AS-79-2004-P
JMH - GA
9 - 25 - 79

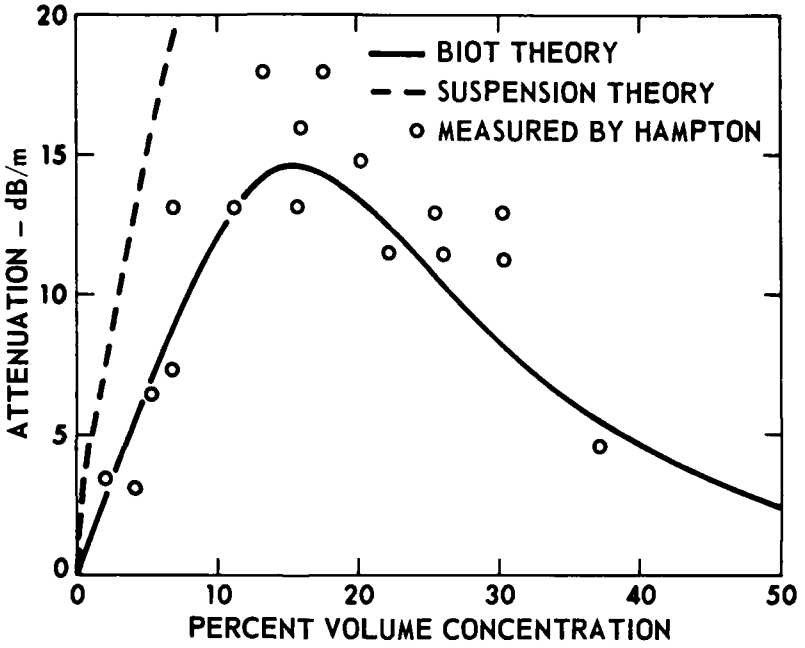

FIGURE 17

COMPRESSIONAL WAVE ATTENUATION AS A FUNCTION OF PARTICLE CONCENTRATION IN KAOLINITE CLAY

PARTICLE DIAMETER = 2 μ

FREQUENCY = 100 kHz

ARL:UT
AS-79-2005-P
JMH - GA
9 - 25 - 79

linearly with frequency and therefore do not necessarily contradict the measurements.

There are two reasons for this. First, even in media of highly uniform grain sizes and shapes there will be a transitional frequency region where the Biot model predicts an increase of attenuation with frequency which is close to linear and this region often happens to coincide with the practical frequencies for laboratory measurements.[10] Second, there is the effect of a distribution in particle sizes. This effect cannot be taken into account by the Biot model since there is only one pore size parameter a_p which determines the frequency dependence. In the suspension model a distribution of sizes can easily be accounted for by simply summing the contributions to the dipole scattering weighted by the relative occurrence of the different sizes. The problem with this model is that it fails when the concentration exceeds a few percent.

Although we do not have any further justification in addition to what has been discussed previously, this shortcoming of the suspension model can partially be overcome by simply multiplying the imaginary part of A in Eq. (40) by a correction factor which depends on the concentration. A possible correction factor is the one given by Eq. (49), which is the ratio between the implied permeability of the suspension model, valid at extremely low concentrations, and the Kozeny-Carman permeability, which is valid at high concentrations.

Figure 18 compares Hampton's measurements of attenuation versus frequency for "black sediment"[33] with the Biot model and the modified suspension model, both using a value of k_o=10. For the modified suspension model Hampton's grain size distribution has been divided into 14 intervals each of width 1ϕ unit covering the interval from 1ϕ to 14ϕ. As can be seen from the figure both models agree quite well with the measurements and could, in fact, be brought to even better agreement with a minor change in the k_o value. A major difference between the two models is the predicted values at lower frequencies. Taking the size distribution into account, the suspension model gives almost a linear dependence on

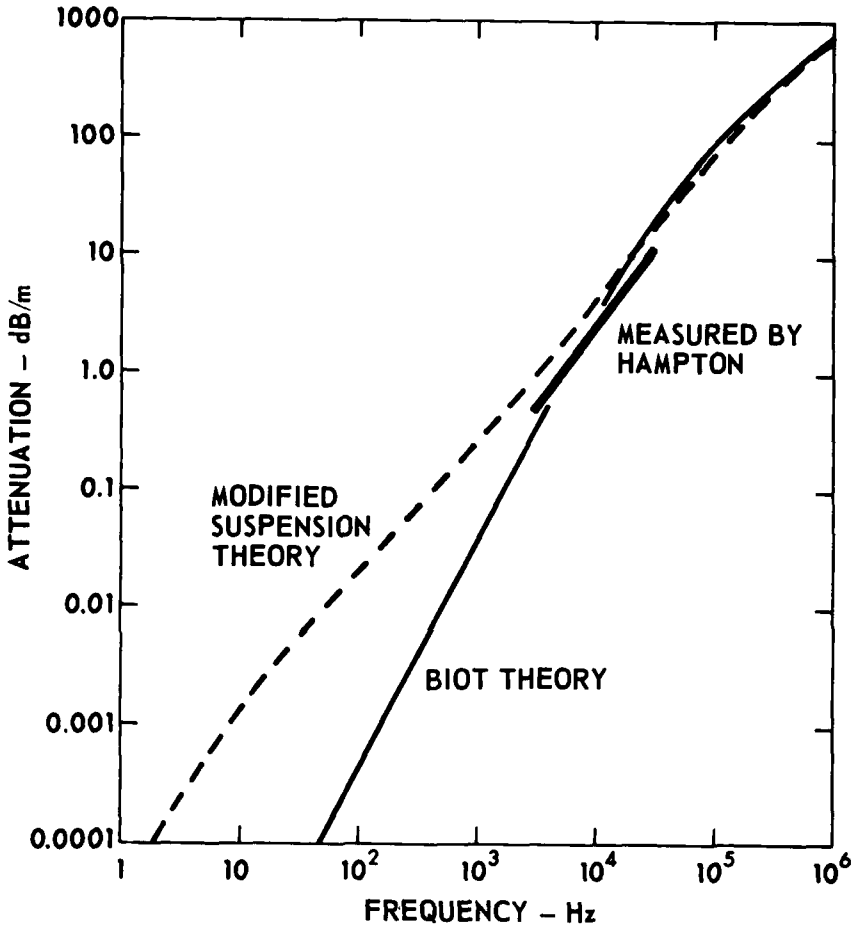

FIGURE 18
COMPRESSIONAL WAVE ATTENUATION AS A FUNCTION OF FREQUENCY FOR A BLACK SOIL SEDIMENT

ARL:UT
AS-79-2006-P
JMH - GA
9 - 25 - 79

frequency, but the Biot model gives a frequency squared dependence at low frequencies; we feel that the frequency behavior of the suspension model is more realistic. This example shows also that theoretical models of viscous attenuation can give a linear increase with frequency.

CONCLUSIONS. We have compared the Biot model and the Urick and Ament model for sound velocity and viscous attenuation in suspensions. It is shown that the models have several common features.

Both theories have been compared with measured attenuation as a function of concentration and it is shown that the Biot model agrees well with the measurements whereas the suspension model fails when the concentration exceeds a few percent. It is concluded that this failure is caused by too simplified a model for the flow resistance of an aggregate of particles. By comparing the two models we have proposed a modification to the suspension model.

A limitation of the Biot model is that it cannot account for the effect of distributed grain sizes, whereas this can be done with the suspension model. It is shown in the suspension model that the result of using a distributed grain size can be a viscous attenuation which increases close to linearly with frequency over a wide frequency range. This suggests that viscous attenuation cannot be computed with any accuracy unless the grain size distribution is known in detail.

Theoretical values for viscous attenuation were compared with a set of measured values for attenuation as a function of frequency. The fairly good agreement suggests that viscous attenuation may also be an important loss mechanism in some silts and clays. The theoretical values, however, assume a permeability which is much higher than the permeability known from soil mechanics.

D. Temperature Dependence of Acoustical Properties of Laboratory Sediments

INTRODUCTION. A study by Shumway[41] showed that the temperature variation of compressional wave speed in marine sediments was dominated by the change with temperature of the pore fluid bulk modulus. Sound speed versus temperature determinations for sea water are therefore commonly used to reduce values of compressional wave speeds of marine sediments to a specified temperature.[30] The correction can be several percent of the total speed. However, compressional wave speed alone is inadequate for a complete acoustic description of sediment acoustic properties; the shear wave speed and the compressional wave and shear wave attenuations are also needed. The variations with temperature of these additional viscoelastic properties have not been studied in detail. This section contains shear wave and compressional wave data measured concurrently as a function of temperature in a water saturated sand sediment and in a water saturated clay sediment. The two diverse types of sediment were selected for study to determine if any of the temperature sensitive acoustic parameters were controlled by grain size or composition.

BACKGROUND. As noted by Shumway,[41] the variation in compressional wave speed with temperature in a saturated sediment should approximately parallel that of the pore fluid alone. This fortuitous relationship is a consequence of the relative magnitudes of the moduli of the sediment constituents and the insensitivity of the sediment grains to small changes in temperature.

Gassman[42] related the compressional wave speed (c_p) in a porous sediment to the moduli of the grain material, the pore fluid, and the sediment framework. He found that

$$c_p^2 = \frac{K + 4\mu/3}{\rho} \quad , \tag{52}$$

$$c_s^2 = \frac{\mu}{\rho} \quad , \tag{53}$$

with

$$K = K_s(K_f+Q)/(K_s+Q) \quad , \tag{54}$$

and

$$Q = K_w(K_s-K_f)/\beta(K_s-K_w) \quad , \tag{55}$$

where β is the sediment porosity, K_w, K_s, and K_f are the bulk moduli of the pore fluid, the solid grain material, and the sediment frame, respectively, and c_s is the shear wave speed. The modulus K_w of the pore fluid can be found by Eq. (52) from a measurement of the density and compressional wave speed in the fluid (the shear modulus, μ, for the fluid would be zero). Since c_p and ρ for a fluid are both functions of temperature, K_w in Eq. (55) is temperature dependent. The bulk modulus of the solid grains, K_s, is, by comparison, independent of temperature. For instance, Brockelsby et al.[43] quote a linear temperature variation of compressional wave speed in fused quartz of 7×10^{-2} m/sec°C. For the temperature range 0-70°C, considered in the present study, the above value would yield a change in speed of approximately 4 m/sec, less than 0.07% of the speed of 5966 m/sec quoted for 20°C. Compared to the average change in speed in pure water over the same temperature range, 2.17 m/sec°C, the effects due to changes in bulk modulus of the grains are insignificant. Shumway[41] presents a graph of the compressibility of water, quartz, and calcite as a function of temperature. The last two are essentially constant.

Shumway[41] neglected the influence of the frame in his calculation of the bulk modulus of a fine sand. If $K_f=0$ in Eq. (54), then

$$K = K_s/[1+\beta(K_s/K_w-1)] \quad . \tag{56}$$

Shumway lacked an experimental value for the rigidity of the sand and instead obtained a value by combining Eq. (52) and Eq. (56) for several different sands. The values obtained gave a reasonable fit to the temperature data. However, the shear modulus so obtained would yield a shear wave speed of approximately 600 m/sec which, in light of shear wave speeds measured since Shumway made his study, is much too high. Equation (56) is inadequate to fit the data in the present study.

Equations (52)-(55) provide an explanation of the constant ratio between the compressional wave speed in water and in sediments. Since K_s is much larger than either K_f or K_w, the temperature variation of Q in Eq. (54) is approximately that of K_w alone. Since K_s is again much larger than Q, the temperature variation is given by that of K_f+Q. If K_f and K_w have approximately the same variation with temperature, then to first approximation K can be written as a constant A times the temperature variation of the fluid, i.e.,

$$K \simeq AK_w(T) \quad . \tag{57}$$

It follows then that the ratio of the sound speed in sediment to that in water can be described by the following approximation.

$$\frac{(c_{sed})^2}{(c_{water})^2} \simeq \frac{AK_w(T) + 4\mu/3}{\rho} \quad \frac{\rho_w}{K_w(T)} \quad . \tag{58}$$

The temperature variation of the densities is small and approximately cancels. Thus, if the shear modulus μ is much smaller than the quantity $AK_w(T)$, then $(c_{sed})^2/(c_{water})^2$ is independent of temperature.

The above explanation is heuristic rather than rigorous, but it does serve to reveal the conditions necessary for the ratio method of temperature compensation to be valid. Both K_w and K_f should be small in comparison to K_s and the temperature variation of K_f should be approximately the same as that of K_w. The value of μ should be small in comparison to K. In the case of surficial marine sediments the above conditions would most probably be met. There are situations, however, when the conditions would not be valid. An example is provided by the data of Timur[44] for the temperature variation of compressional wave speeds in saturated porous rocks subject to large confining pressures. In that case, both μ and K_f are large. Experimentally, the compressional wave speed decreases with an increase in temperature.

The object of the work described here was to examine the temperature dependence of the shear modulus and frame bulk modulus of highly unconsolidated water saturated sediments. Although there is a large amount of data in the literature for compressional waves in consolidated and unconsolidated media and for shear waves in consolidated media, there is a lack of valid data for shear waves in unconsolidated media due in most part to the difficulty in generating and detecting the waves in such a highly attenuating medium. Shirley et al.[8,19] have developed a method for measuring shear waves based on the ceramic bender transducer which allows measurements in highly unconsolidated media with shear moduli as low as 5.5×10^4 dyn/cm^2.[8]

In the above discussion, elastic wave propagation has been assumed and effects due to viscoelastic properties of the medium have been ignored. However, there are dissipative mechanisms operating on both types of acoustic waves in a sediment and if these mechanisms have an appreciable dependence upon temperature, the relationship discussed above would be altered. Attenuation measurements of both compressional waves and shear waves were thus also incorporated in the present study.

EXPERIMENTAL PROCEDURE. The acoustic parameter values of a water saturated, mature, medium quartz beach sand from Panama City, Florida, and of a water saturated kaolinite clay from the Georgia Kaolin Company were obtained by standard pulse transmission techniques. Different sets of transducers were used for the clay measurements and for the sand. The different transducers were basically similar. Each consisted of a bender transducer element for shear wave measurements and a small compressional wave element bonded together in plastic. (Similar type transducers have been described previously.[19]) The measurement technique utilized a three-transducer arrangement with one projector and two receivers. The three transducers were immersed in the sediment with the two receivers at slightly different spacing from the projector. Spacing between the two receivers was measured by observing the travel time for pulses in pure water and using handbook values for speed to calculate separation. Amplitude response as a function of temperature was also measured for each of the receivers in pure water. Calibration for the shear wave

measurements required additional steps since the comparison with water used for compressional waves is not possible. For shear wave speed measurements, the separation found for the compressional wave elements was assumed for the shear wave elements since the two are rigidly bonded together. Dry sand was used for amplitude calibration of the shear wave elements with temperature since temperature effects are expected to be nominal for the dry material. Temperature of the sediment samples was controlled by a circulating thermostatic bath using copper tubing coiled around the insulated sample chamber. Temperature was measured by a digital quartz thermometer.

The sediments were prepared for use by first wetting the dry material with deionized water, boiling the mixture, and then subjecting the sediment to a vacuum for a minimum of 24 hours. In the case of the sand, the sample chamber was vibrated for several minutes and allowed to stand overnight to obtain a stable packing. The final porosity of the sand was approximately 0.386. For the clay, the mixture was placed in the sample chamber and allowed to stand for one week in order to approach a constant porosity of about 0.75. In both cases, the transducers were approximately 16 cm below the sediment surface.

COMPRESSIONAL WAVE SPEED. Figure 19 shows the observed variation with temperature of the compressional wave speed in both pure water and in water saturated sand. The solid line drawn through the data points for the sand is the expected speed dependence using the ratio method[30] in which the ratio of the speed in sediment and in water is found at a particular temperature (usually room temperature), and the speed in sediment as a function of temperature is calculated by applying the same ratio to speeds for water. As expected, the variation approximately parallels that in the pore fluid alone. The plotted data are the result of measurements over several cycles of raising and lowering the sediment temperature. Figure 20 displays the results of measurements of the compressional wave parameters in the clay. Again the results tend to confirm previous work. In the case of the clay, the compressional wave speed in the sediment is lower than that in water due to the high porosity of the sediment--a result predicted by Wood for suspensions of particles.[45]

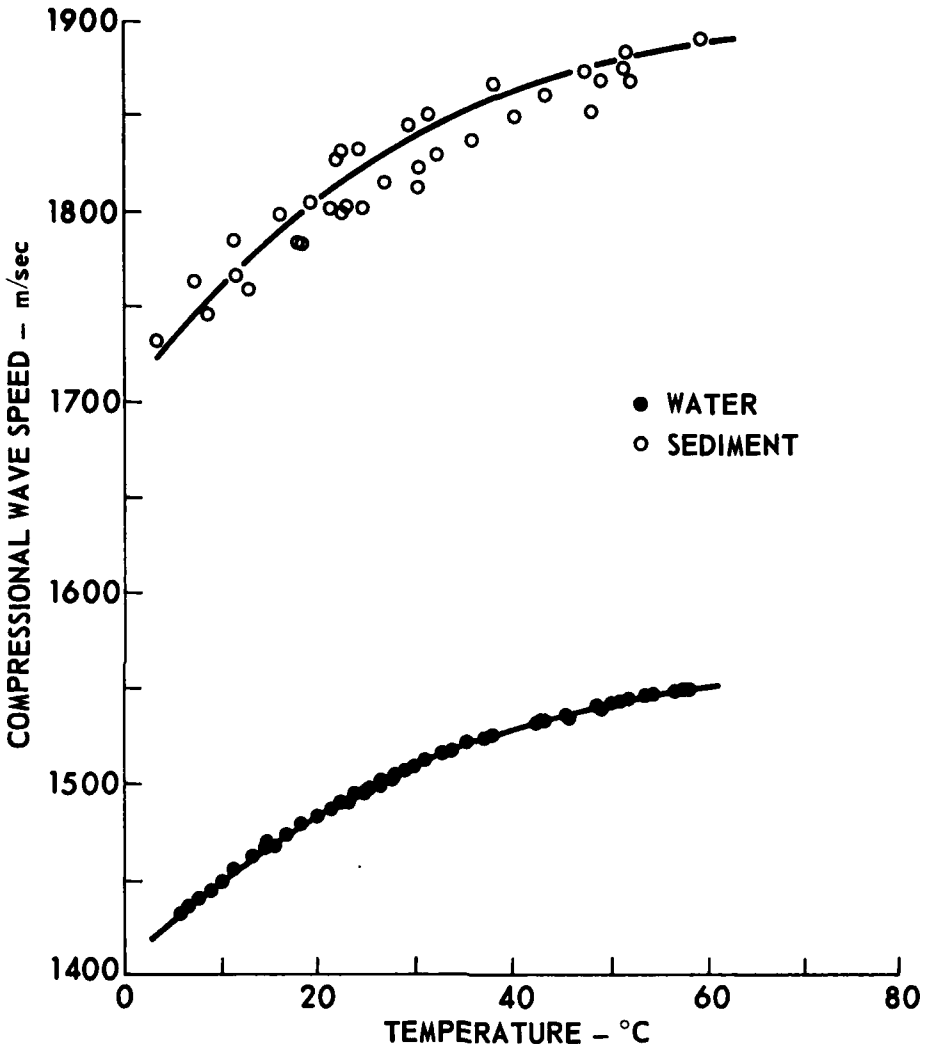

FIGURE 19
COMPRESSIONAL WAVE SPEED AS A FUNCTION OF TEMPERATURE
IN WATER AND IN WATER SATURATED SAND SEDIMENT

ARL:UT
AS-79-2183-S
DJS - GA
11 - 6 - 79

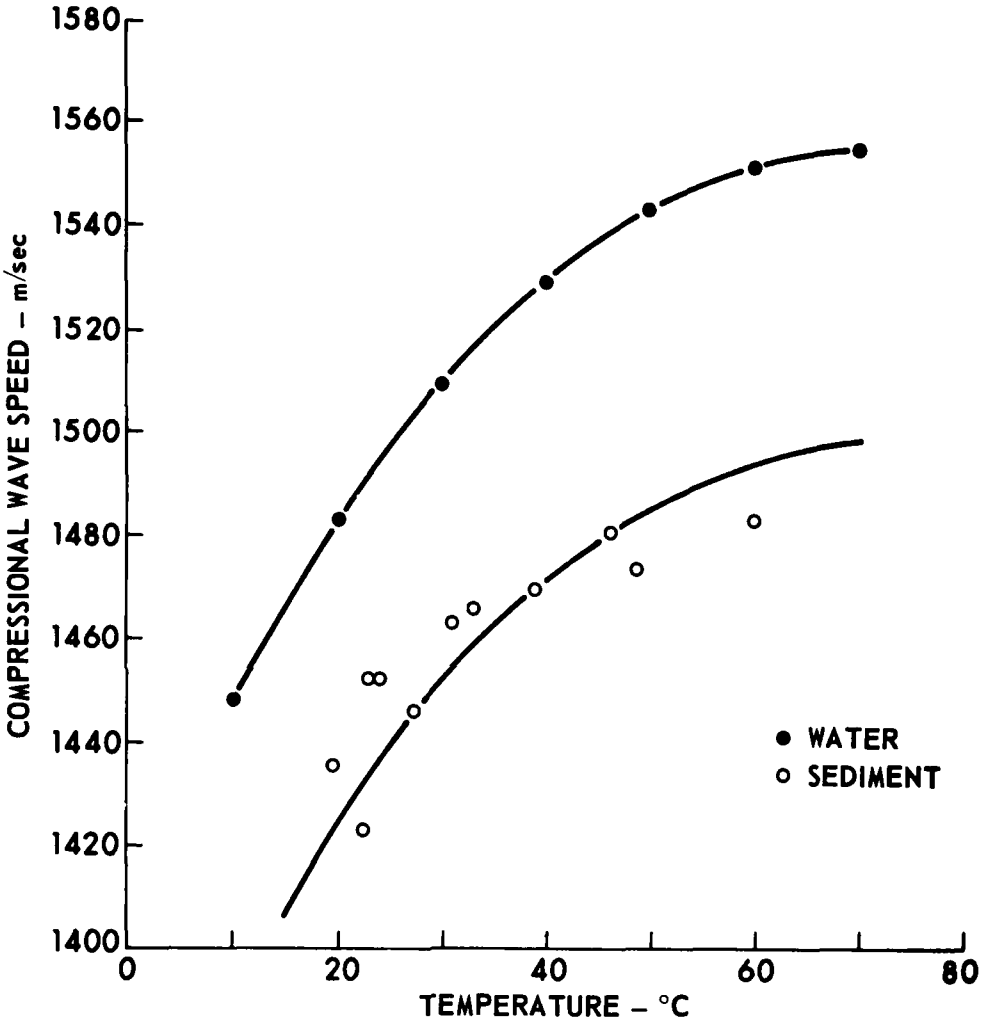

FIGURE 20
COMPRESSIONAL WAVE SPEED AS A FUNCTION OF TEMPERATURE
IN WATER AND IN WATER SATURATED KAOLINITE CLAY SEDIMENT

ARL:UT
AS-79-2188-S
DJS - GA
11 - 6 - 79

SHEAR WAVE SPEED. Figure 21 shows the variation with temperature observed for the shear wave speed in sand. There are two sets of data displayed, both obtained in the same sediment. The data marked "unlined" exhibit a significant decrease in speed with increased temperature. It was postulated that some of the change could be due to changes in strain supplied by expansion and contraction of the walls of the sample chamber. For the temperature range under investigation, the expected change in diameter of the cylindrical aluminum chamber was calculated to be approximately one grain size (0.35 mm) out of 600 grain size total.

The experiment was repeated with a 2.54 cm thick layer of water filled polyurethane foam placed on the inside surface of the container to form a pressure release between the metal walls and the sediment. The data set marked "lined" in Fig. 21 was then obtained and shows an essentially constant shear wave speed over the whole temperature range. The two lines in the figure are least squares fits to each data set. The slight increase in slope exhibited by the second data set is more likely due to settling of the sand as the experiment progressed since the higher velocity data were obtained at a later time than the lower velocity data.

Figure 22 shows the shear wave speed data measured for the kaolinite clay. In this experiment a foam liner was initially placed in the sediment container to eliminate the problems encountered with the sand. The change in speed is again within experimental error over the entire temperature range.

BULK MODULI. The concurrent measurement of compressional wave and shear wave speeds enabled calculation of the component bulk moduli of the sediment from Eqs. (52)-(55). Figure 23 shows the data obtained for the sand. The data marked sediment, water, and frame are the three bulk moduli K, K_w, and K_f, respectively. The frame bulk modulus K_f contributes significantly to the overall sediment compressibility (see Eq. (54)) and apparently also varies slightly with temperature in about the same proportion as K_w.

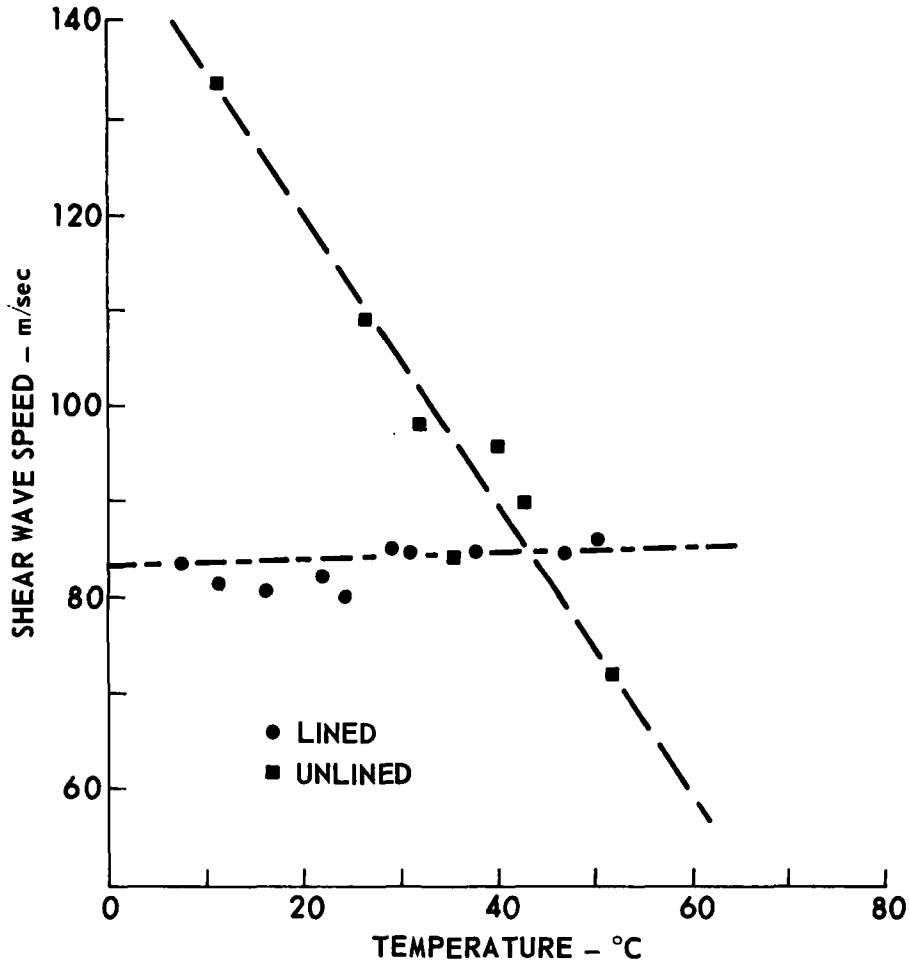

FIGURE 21
SHEAR WAVE SPEED AS A FUNCTION OF TEMPERATURE
IN WATER SATURATED SAND SEDIMENT

ARL:UT
AS-79-2184-S
DJS - GA
11 - 6 - 79

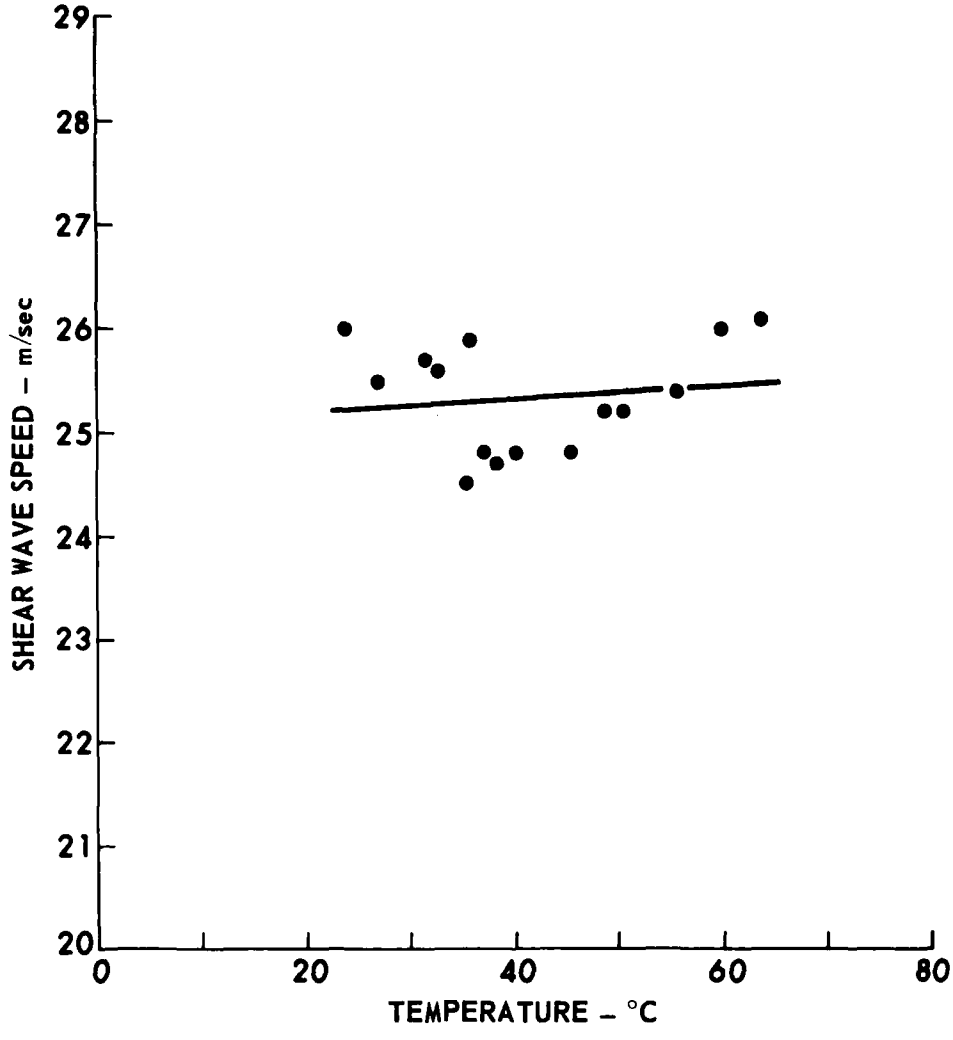

FIGURE 22
SHEAR WAVE SPEED AS A FUNCTION OF TEMPERATURE
IN WATER SATURATED KAOLINITE CLAY SEDIMENT

ARL:UT
AS-79-2185-S
DJS - GA
11 - 6 - 79

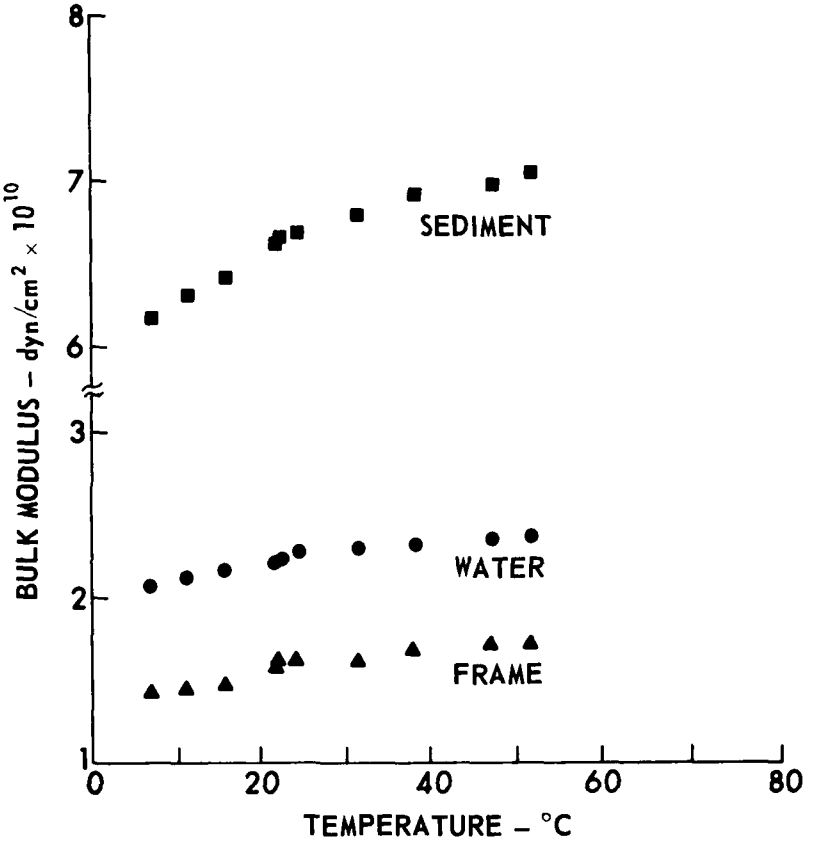

FIGURE 23
COMPONENT BULK MODULI AS A FUNCTION OF TEMPERATURE FOR WATER SATURATED SAND SEDIMENT

ARL:UT
AS-79-2182-S
DJS - GA
11 - 6 - 79

Figure 24 displays the component bulk moduli calculated from the compressional wave and shear wave data for kaolinite clay. The frame modulus for this case is relatively small and contributes very little to the total sediment bulk modulus. Also, the frame bulk modulus seemingly does not vary with temperature so that the sediment bulk modulus parallels the pore fluid bulk modulus in temperature response.

COMPRESSIONAL WAVE ATTENUATION. Figure 25 shows the variation with temperature of the relative amplitudes of the signals at the two receivers. Since the attenuation of sound in water is negligible, values obtained in water represent the geometric divergence of the energy and the change with temperature of the transducer amplitude responses. The solid lines in Fig. 25 are linear regression values for each data set and, since the two lines do not diverge, the indication is that the attenuation does not vary with temperature. The average attenuation calculated from the data is 218 ±25 dB/m at 700 kHz.

Figure 26 shows the amplitude data obtained for the kaolinite clay. Since different transducers were used for the clay data, the response to temperature is different from that of the sand. The linear regression lines for water and clay fall almost together indicating a low value of attenuation for the clay. Previous measurements of compressional wave attenuation in kaolinite clay at 0.75 porosity show values of about 1 to 10 dB/m at 120 kHz.[1] Such a low value is less than the measurement error for this case. Again, there is no appreciable change in the attenuation in the clay as temperature is varied.

SHEAR WAVE ATTENUATION. Shear wave attenuation measurements were made only on the kaolinite clay. Figure 27 displays the amplitude response of the shear wave transducers as a function of temperature for clay and for dry sand. The values for dry sand are offset downward by 10 dB to clarify the illustration and are included only as a comparison to the clay data to show that the temperature response is the same in both cases. Dry sand was chosen for comparison because the temperature response in a dry sand due to grain-to-grain friction is expected to be small. The mechanisms

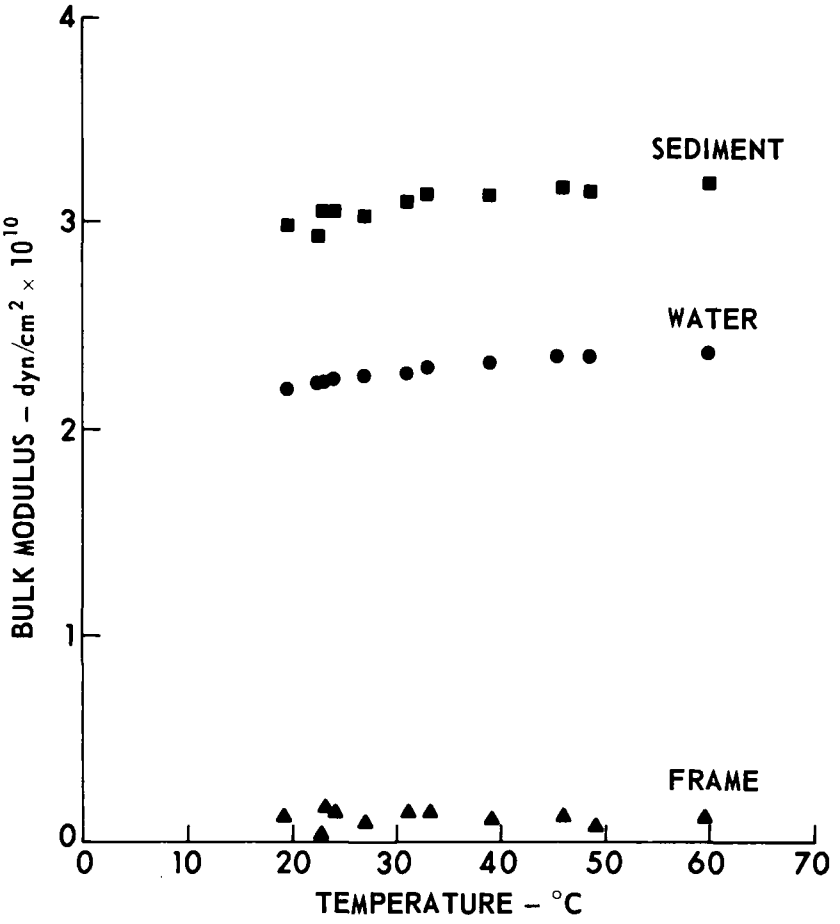

FIGURE 24
COMPONENT BULK MODULI AS A FUNCTION
OF TEMPERATURE FOR WATER SATURATED
KAOLINITE CLAY SEDIMENT

ARL:UT
AS-79-2193-S
DJS- GA
11- 12-79

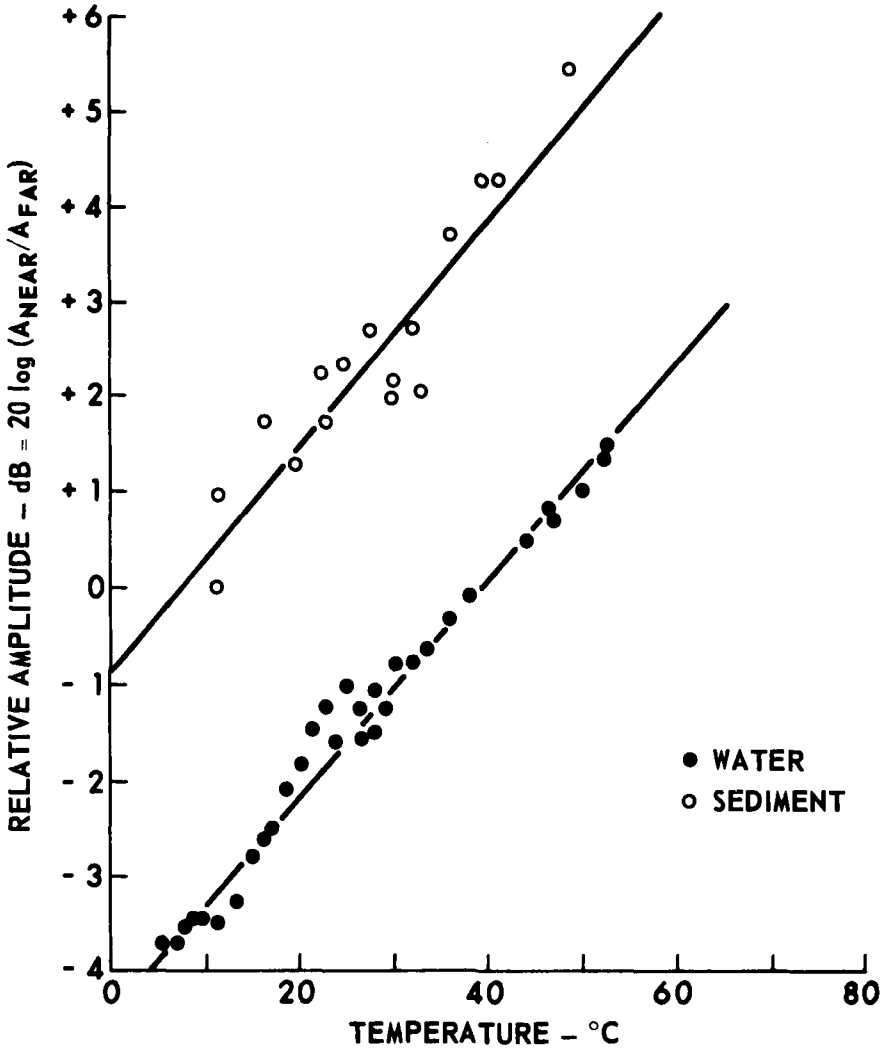

FIGURE 25
RELATIVE SIGNAL AMPLITUDES AS A FUNCTION OF TEMPERATURE IN WATER AND IN WATER SATURATED SAND SEDIMENT FOR COMPRESSIONAL WAVES

ARL:UT
AS-79-2187-S
DJS - GA
11 - 6 - 79

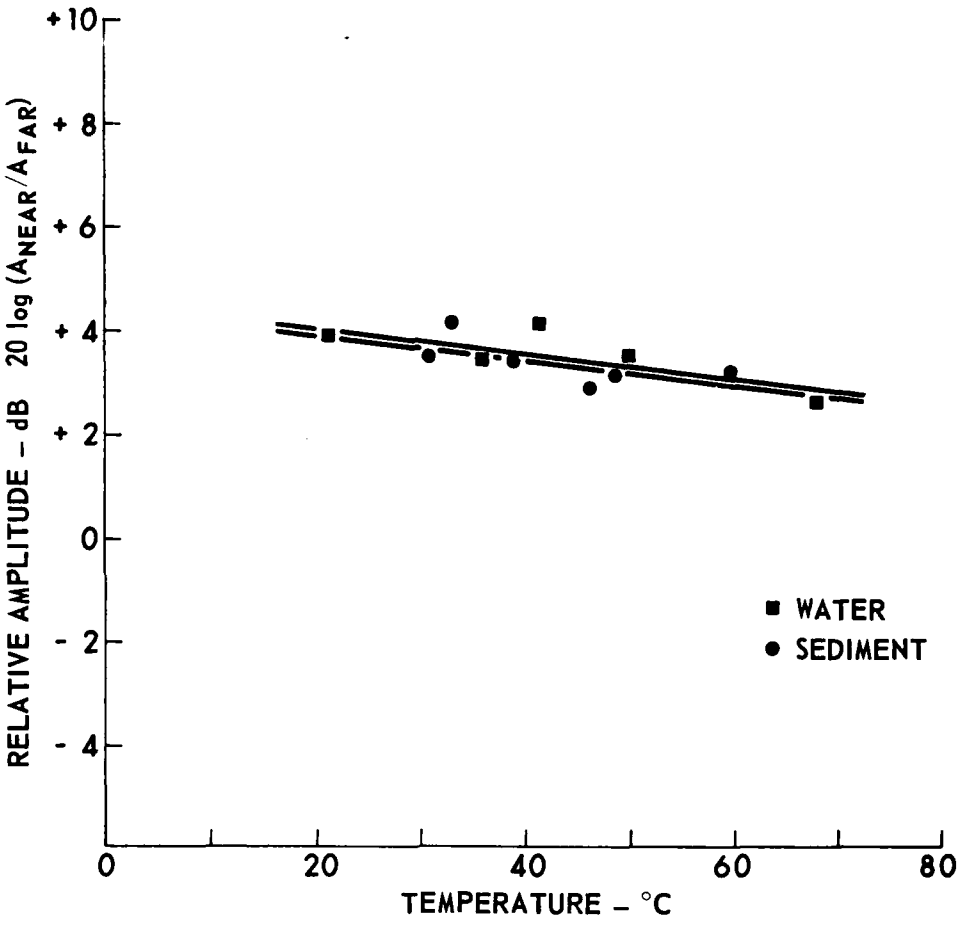

FIGURE 26
RELATIVE SIGNAL AMPLITUDES AS A FUNCTION OF TEMPERATURE IN WATER AND IN WATER SATURATED KAOLINITE CLAY SEDIMENT FOR COMPRESSIONAL WAVES

ARL:UT
AS-79-2186-S
DJS- GA
11- 6-79

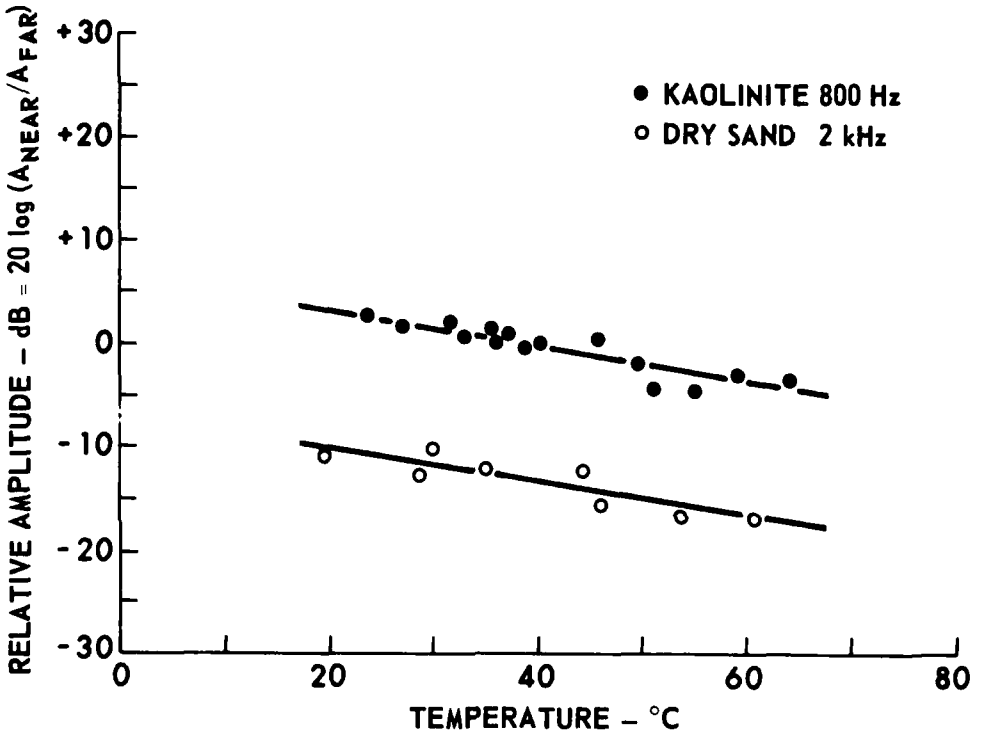

FIGURE 27
RELATIVE SIGNAL AMPLITUDES AS A FUNCTION OF TEMPERATURE IN DRY SAND AND IN WATER SATURATED KAOLINITE CLAY FOR SHEAR WAVES

ARL:UT
AS-79-2189-S
DJS - GA
11 - 6 - 79

responsible for attenuation are different for dry sand and for saturated clay. Since the absolute attenuation value for the dry sand was not known, the absolute value of attenuation in the clay cannot be obtained from the data in Fig. 27. Previous measurements, however, indicate that kaolinite clay at 0.75 porosity should have a shear wave attenuation of about 100 dB/m.[8]

DISCUSSION AND CONCLUSIONS. The data presented in this paper illustrate the usefulness of concurrent measurements of compressional wave and shear wave properties in unconsolidated sediments. Even in the highly porous clay material, there is enough rigidity to enable the propagation of a significant amount of shear wave energy. The following conclusions can be drawn from the data for low amplitude acoustic waves in saturated sand and clay sediments:

(1) the shear wave speed is independent of temperature,

(2) the compressional wave speed varies significantly with temperature, but can be extrapolated between temperatures if the speed in the pore fluid is known as a function of temperature, and

(3) the compressional wave and shear wave attenuation are also insensitive to temperature.

Additional work is needed before the above results can confidently be applied to other sediment types.

IV. SUMMARY

During the past year, the ARL:UT sediment acoustics program progressed in three areas.

(1) Three field trips were made, two successfully completed, on which five in situ compressional wave speed profiles were made adding to the growing base of in situ compressional wave data for various areas of the world. Four profiles were made in the Gulf of Mexico and one in the Caribbean Sea.

(2) A test using a shear wave transducer to obtain an in situ shear speed profile was accomplished. Although the data are not as good as analogous compressional wave data, it does show that such data can be obtained.

(3) Analytical models using only easily measured physical parameters have been successfully developed for compressional wave propagation in porous media (such as sands). These models are based on those of Biot and Stoll, with some extension to fine grain clay type sediments. Model predictions were compared to laboratory data and show good agreement. Studies of temperature effects on shear wave and compressional wave propagation in sands and clays were successfully carried out and show that previously unsubstantiated assumptions about temperature dependence are essentially correct.

Future work under the program will concentrate on laboratory measurements with attention focused on low frequency acoustic propagation. Topics include:

1. theoretical model development,
2. physical scale model development,
3. investigation of interface waves,
4. investigation of nonlinear acoustic parameters of sediments,
5. examination of Biot's second type of compressional wave,
6. effects of salinity on sediment acoustic properties, and
7. backscattering of shear waves.

REFERENCES

1. A. L. Anderson, "Acoustics of Gas-Bearing Sediments," Applied Research Laboratories Technical Report No. 74-19 (ARL-TR-74-19), Applied Research Laboratories, The University of Texas at Austin, Austin, Texas, May 1974.

2. D. J. Shirley and A. L. Anderson, "In Situ Measurement of Marine Sediment Acoustical Properties During Coring in Deep Water," IEEE Trans. Geoscience Electronics GE-13, No. 4 (1975).

3. "Status Report No. 1 under Texas A&M Research Foundation, P.O. No. RF-11743, and under ONR Contract N00014-70-A-0166, Task 0005," Applied Research Laboratories, The University of Texas at Austin, 7 July 1971.

4. D. J. Shirley, A. L. Anderson, and L. D. Hampton, "In Situ Measurement of Sediment Sound Speed During Coring," Applied Research Laboratories Technical Report No. 73-1 (ARL-TR-73-1), Applied Research Laboratories, The University of Texas at Austin, 14 March 1973.

5. D. J. Shirley and A. L. Anderson, "Compressional Wave Profilometer for Deep Water Measurements," Applied Research Laboratories Technical Report No. 74-51 (ARL-TR-74-51), Applied Research Laboratories, The University of Texas at Austin, 6 December 1974.

6. D. J. Shirley and A. L. Anderson, "Studies of Sediment Shear Waves, Acoustical Impedance, and Engineering Properties," Applied Research Laboratories Technical Report No. 75-23 (ARL-TR-75-23), Applied Research Laboratories, The University of Texas at Austin, 7 May 1975.

7. D. J. Shirley and D. W. Bell, "Acoustics of In Situ and Laboratory Sediments," Applied Research Laboratories Technical Report No. 78-36 ARL-TR-78-36), Applied Research Laboratories, The University of Texas at Austin, 14 August 1979.

8. D. J. Shirley and L. D. Hampton, "Shear wave measurements in laboratory sediments," J. Acoust. Soc. Am. 63, 607-613 (1978).

9. D. J. Shirley, "Method for measuring in situ acoustic dependence of marine sediments," J. Acoust. Soc. Am. 62, 1028-1032 (1977).

10. J. M. Hovem and G. D. Ingram, "Viscous attenuation of sound in saturated sand," J. Acoust. Soc. Am. 66, 1807-1812 (1979).

11. J. M. Hovem, "Viscous attenuation of sound in suspensions and high porosity marine sediments," accepted for publication in The Journal of the Acoustical Society of America (1979).

12. D. W. Bell and D. J. Shirley, "Temperature variation of the acoustical properties of laboratory sediments," submitted for publication in The Journal of the Acoustical Society of America (January 1980).

13. D. J. Shirley, D. W. Bell and J. M. Hovem, "Laboratory and Field Studies of Sediment Acoustics," Applied Research Laboratories Technical Report No. 79-26 (ARL-TR-79-26), Applied Research Laboratories, The University of Texas at Austin, 12 June 1979.

14. D. W. Bell, "Shear Wave Propagation in Unconsolidated Fluid Saturated Porous Media," Applied Research Laboratories Technical Report No. 79-31 (ARL-TR-79-31), Applied Research Laboratories, The University of Texas at Austin, 15 May 1979.

15. J. M. Hovem, "Some Aspects of Sound Propagation in Saturated Sand," presented at the Seminar on Bottom Effects in Underwater Sound Propagation, Miami, Florida, April 1979.

16. J. M. Hovem, "Finite Amplitude Effects in Marine Sediments," presented at the Conference on Underwater Applications of Nonlinear Acoustics, University of Bath, Bath, England, September 1979.

17. D. J. Shirley and D. W. Bell, "Temperature variation of the acoustic properties of laboratory sediments," presented at the 98th Meeting of the Acoustical Society of America, Salt Lake City, Utah, November 1979.

18. D. J. Shirley, "Laboratory and In Situ Sediment Acoustics," Applied Research Laboratories Technical Report No. 77-46 (ARL-TR-77-46), Applied Research Laboratories, The University of Texas at Austin, 23 August 1977.

19. D. J. Shirley, "An improved shear wave transducer," J. Acoust. Soc. Am. 63, 1643-1645, May 1978.

20. M. A. Biot, "Theory of propagation of elastic waves in a fluid-saturated porous solid, I. Low-frequency range," J. Acoust. Soc. Am. 28, 168-178 (1956).

21. M. A. Biot, "Theory of propagation of elastic waves in a fluid-saturated porous solid, II. Higher frequency range," J. Acoust. Soc. Am. 28, 179-191 (1956).

22. M. A. Biot, "Generalized theory of acoustic propagation on porous dissipative media," J. Acoust. Soc. Am. 34, 1254-1264 (1962).

23. R. D. Stoll and G. M. Bryan, "Wave attenuation in saturated sediments," J. Acoust. Soc. Am. 47, 1440-1447 (1969).

24. R. D. Stoll, "Acoustic waves in saturated sediments," in Physics of Sound in Marine Sediments, edited by L. D. Hampton (Plenum Press, New York, 1974).

25. R. D. Stoll, "Acoustic waves in ocean sediments," Geophys. 42, 715-725 (1977).

26. P. C. Carman, Flow of Gases through Porous Media, (Academic Press, New York, 1956).

27. J. F. Mifsud, "Experimental Study of the Acoustic Properties of Water-Filled Sands," Defense Research Laboratory Acoustical Report No. 72 (DRL-A-72), Defense Research Laboratory, The University of Texas, Austin, Texas, 1953.

28. A. W. Nolle, W. A. Hoyer, J. F. Mifsud, W. R. Runyan, and M. A. Ward, "Acoustical properties of water-filled sands," J. Acoust. Soc. Am. 35, 1394-1408 (1963).

29. T. Geertsma and D. C. Smit, "Some aspects of elastic wave propagation in fluid-saturated porous solids," Geophys. 26, 169-181 (1961).

30. E. L. Hamilton, "Elastic properties of marine sediments," J. Geophys. Res. 76, 579-604 (1971).

31. S. N. Domenico, "Elastic properties of unconsolidated porous sand reservoirs," Geophys. 42, 1339-1368 (1977).

32. The experimental expression relating attenuation (in N/cm) and mean grain size radius a (cm) is given as $\alpha=3.7\times15^{-7}(\omega^{1/2}a)$, but in Fig. 3 of Ref. 10 and in the original report by Mifsud[9] the empirical coefficient is given as 5.4×10^{-7}. We have concluded that Eq. (11) of Ref. 10 is a misprint and therefore we have used $\alpha=5.4\times10^{-7}$ $(\omega^{1/2}a)$ in our discussion.

33. L. D. Hampton, "Acoustic properties of sediments," J. Acoust. Soc. Am. 42, 882-890 (1967).

34. E. L. Hamilton, "Compressional-wave attenuation in marine sediments," Geophys. 37, 620-646 (1972).

35. R. J. Urick, "The absorption of sound in suspensions of irregular particles," J. Acoust. Soc. Am. 20, 283-289 (1948).

36. R. J. Urick and W. S. Ament, "The propagation of sound in composite media," J. Acoust. Soc. Am. 21, 115-119 (1949).

37. W. R. Bryant, A. P. Deflache, and P. K. Trabant, "Consolidation of marine clays and carbonates," in Deep-Sea Sediments, Physical and Mechanical Properties, edited by A. L. Inderbitzen (Plenum Press, New York, 1974), pp. 209-244.

38. P. G. Waterman and R. Truell, "Multiple scattering of waves," J. Math. Phys. 2, 512-537 (1961).

39. Following Hampton we have concluded that the attenuation values given by Urick in his Fig. 5 (Ref. 7) are ten times too high due to misprints on the vertical axes.

40. C. McCann, "Compressional wave attenuation in concentrated clay suspensions," Acustica 22, 352-356 (1969-70).

41. G. Shumway, "Sound velocity versus temperature in water-saturated sediments," Geophysics 23, 494-505 (1958).

42. F. Gassman, "Elastic waves through a packing of spheres," Geophysics 16, 673-685 (1951).

43. C. F. Brockelsby, J. S. Palfreeman, and D. Gilson, Ultrasonic Delay Lines (Iliffe, London, 1963).

44. A. Timur, "Temperature dependence of compressional and shear wave velocities in rocks," Geophysics 42, 950-956 (1977).

45. A. B. Wood, A Textbook of Sound, 3rd ed., 1955 (McGraw-Hill, New York, 1930).

APPENDIX
BIBLIOGRAPHY OF
ONR CODE 480 PROGRAM
DOCUMENTATION

Addy, S. R., E. W. Behrens, T. R. Haines, D. J. Shirley and J. L. Worzel, "Correlation of Some Lithologic and Physical Characteristics of Sediments with High Frequency Subbottom Reflection Types," Proceedings of the 11th Annual Offshore Technology Conference, Houston, Texas, 30 April - 3 May 1979.

Anderson, A. L., and L. D. Hampton, "In Situ Measurement of Sediment Acoustic Properties During Coring," presented at the ONR Symposium on Physical and Engineering Properties of Deep-Sea Sediments, Airlie House, Airlie, Virginia, 24-27 April 1973.

Anderson, A. L., and L. D. Hampton, "Measurement of In Situ Acoustic Properties During Sediment Coring," paper presented at the ONR Symposium on the Physics of Sound In Marine Sediments, Lakeway Inn, Austin, Texas, 8-10 May 1973.

Anderson, A. L., and L. D. Hampton, "In Situ Measurements of Sediment Acoustic Properties During Coring," In Deep-Sea Sediments, Physical and Mechanical Properties, edited by A. L. Inderbitzen (Plenum Press, New York, 1974).

Anderson, A. L., "Acoustics of Gas-Bearing Sediments," Applied Research Laboratories Technical Report No. 74-19 (ARL-TR-74-19), Applied Research Laboratories, The University of Texas at Austin, May 1974.

Anderson, A. L., and L. D. Hampton, "A Method for Measuring In Situ Acoustic Properties During Sediment Coring," In Physics of Sound in Marine Sediments, edited by Loyd Hampton (Plenum Press, New York, 1974)

Anderson, A. L., and L. D. Hampton, "Use of Tubes for Measurement of Acoustical Properties of Materials," presented at the 89th Meeting of the Acoustical Society of America, Austin, Texas, April 1975.

Anderson, A. L., R. J. Harwood, and L. D. Hampton, "Temperature Studies on Lake Travis Stratification in a Warm Monomictic Reservoir," The Texas Journal of Science XXVI, Nos. 3 and 4, 353-371, August 1975.

Ellis, G. E., "Summary of Environmental Acoustic Data Processing," Final Report under Contract N00014-70-A-0166, Task 0019, 1 September - 31 December 1973, Applied Research Laboratories Technical Report No. 75-32 (ARL-TR-75-32), Applied Research Laboratories, The University of Texas at Austin, June 1975.

Ellis, G. E., "Summary of Environmental Acoustic Data Processing, Annual Report nder Contract N00014-70-A-0166, Task 0016, 1 July 1973 - 30 June 1974," Applied Research Laboratories Technical Report No. 76-31 (ARL-TR-76-31), Applied Research Laboratories, The University of Texas at Austin, July 1976.

Hampton, L. D., "ARL Experience with Acoustics and Gas in Sediments," presented at Symposium on Natural Gases in Marine Sediments and Their Mode of Distribution, The University of California, Lake Arrowhead Conference Center, Lake Arrowhead, California, 28-30 November 1972.

Hampton, L. D., and A. L. Anderson, "Acoustics and Gas in Sediments: Applied Research Laboratories (ARL) Experience," in Natural Gases in Marine Sediments, Marine Science, Vol. III, edited by Isaac R. Kaplan (Plenum Press, New York, 1974).

Hovem, J. M., "Some Aspects of Sound Propagation in Saturated Sand," presented at the Seminar on Bottom Effects in Underwater Sound Propagation, Miami, Florida, April 1979.

Hovem, J. M., "The Nonlinearity Parameter of Saturated Marine Sediments," scheduled to appear in The Journal of The Acoustical Society of America, November 1979. (ARL-TP-79-17, rev., May 1979).

Hovem, J. M., "Finite Amplitude Effects in Marine Sediments," presented at the Conference on Underwater Applications of Nonlinear Acoustics, University of Bath, Bath, England, September 1979. (ARL-TP-79-41, June 1979).

Hovem, J. M., "Viscous Attenuation of Sound in Suspensions and High Porosity Marine Sediments," submitted to The Journal of The Acoustical Society of America. (ARL-TP-79-62, September 1979).

Hovem, J. M., and G. D. Ingram, "Viscous Attenuation of Sound in Saturated Sand," scheduled to appear in The Journal of The Acoustical Society of America, December 1979. (ARL-TP-79-35, April 1979).

Kibblewhite, A. C., "Attenuation of Underwater Sound of Low Frequencies," Applied Research Laboratories Technical Report No. 76-1 (ARL-TR-76-1), Applied Research Laboratories, The University of Texas at Austin, December 1975.

Shirley, D. J., "Final Report under Contract N00014-70-A-0166, Task 0005," Applied Research Laboratories Technical Report No. 72-6 (ARL-TR-72-6), Applied Research Laboratories, The University of Texas at Austin, January 1972.

Shirley, D. J., and L. D. Hampton, "Acoustic Velocity Profilometer for Sediment Cores," OCEAN '72, Record of the International Conference on Engineering in the Ocean Environment, Newport, Rhode Island, 13-15 September 1972.

Shirley, D. J., and A. L. Anderson, "Experimental Investigation of Shear Waves in Laboratory Sediments," presented at the 90th Meeting of the Acoustical Society of America, San Francisco, California, 3-7 November 1975.

Shirley, D. J., "Determination of the Acoustic Properties of Deep Ocean Sediments from In Situ Profiles," presented at the 92nd Meeting of The Acoustical Society of America, San Diego, California, 15-19 November 1976.

Shirley, D. J., and A. L. Anderson, "Shear Waves in Unconsolidated Sediments," presented at the 92nd Meeting of The Acoustical Society of America, San Diego, California, 15-19 November 1976.

Shirley, D. J., "Acoustic Impedance Measuring Device for Marine Sediments," presented at the 93rd Meeting of The Acoustical Society of America, University Park, Pennsylvania, 6-10 June 1977.

Shirley, D. J., "Laboratory and In Situ Sediment Acoustics," Applied Research Laboratories Technical Report No. 77-46 (ARL-TR-77-46), Applied Research Laboratories, The University of Texas at Austin, August 1977.

Shirley, D. J., "Method for Measuring In Situ Acoustic Impedance of Marine Sediments," J. Acoust. Soc. Am. 62, 1028-1032 (October 1977).

Shirley, D. J., and L. D. Hampton, "Shear Wave Measurements in Laboratory Sediments," J. Acoust. Soc. Am. 63, 607-613, February 1978.

Shirley, D. J., "An Improved Shear Wave Transducer," J. Acoust. Soc. Am. 63, 1643 (1978).

Shirley, D. J., "Development of a Bottom Hole Device for Offshore Shear Wave Velocity Measurement," Proceedings of the 10th Annual Offshore Technology Conference, Houston, Texas, 8-11 May 1978.

Shirley, D. J., and D. W. Bell, "Acoustics of In Situ and Laboratory Sediments," Applied Research Laboratories Technical Report No. 78-36 (ARL-TR-78-36), Applied Research Laboratories, The University of Texas at Austin, August 1978.

Shirley, D. J., and D. W. Bell, "Temperature Variation of the Acoustic Properties of Laboratory Sediments," presented at the 98th Meeting of The Acoustical Society of America, Salt Lake City, Utah, November 1979.

"Status Report No. 1 under Texas A&M Research Foundation, P. O. No. RF-11743 and ONR Contract N00014-70-A-0166, Task 0005," 1 January - 1 July 1971, July 1971.

Shirley, D. J., and L. D. Hampton, "Determination of Sound Speed in Cored Sediments," Applied Research Laboratories Technical Report No. 72-44 (ARL-TR-72-44), Applied Research Laboratories, The University of Texas at Austin, December 1972.

Shirley, D. J., A. L. Anderson, and L. D. Hampton, "In Situ Measurement of Sediment Sound Speed During Coring," Applied Research Laboratories Technical Report No. 73-1 (ARL-TR-73-1), Applied Research Laboratories, The University of Texas at Austin, March 1973.

Shirley, D. J., A. L. Anderson, and L. D. Hampton, "Measurement of In Situ Speed During Sediment Coring," OCEAN '73, Record of the International Conference on Engineering in the Ocean Environment, Seattle, Washington, 25-28 September 1973.

Shirley, D. J., and L. D. Hampton, "Acoustic Velocimeter for Ocean Bottom Coring Apparatus," ARL Invention Disclosure, November 1973.

Shirley, D. J., "Interim Technical Description of the ARL Compressional Wave In Situ Core Profilometer," Applied Research Laboratories Technical Memorandum No. 74-9 (ARL-TM-74-9), Applied Research Laboratories, The University of Texas at Austin, March 1974.

Shirley, D. J., "Calibration Manual for ARL Profilometer," Informal Memorandum, July 1974.

Shirley, D. J., and A. L. Anderson, "Compressional Wave Profilometer for Deep Water Measurements," Applied Research Laboratories Technical Report No. 74-51 (ARL-TR-74-51), Applied Research Laboratories, The University of Texas at Austin, December 1974.

Shirley, D. J., "Fine Structure of the Sound Speed Profile in Ocean Bottom Sediments," presented at the 89th Meeting of the Acoustical Society of America, Austin, Texas, 7-11 April 1975.

Shirley, D. J., and A. L. Anderson, "Studies of Sediment Shear Waves, Acoustical Impedance, and Engineering Properties," Applied Research Laboratories Technical Report No. 75-23 (ARL-TR-75-23), Applied Research Laboratories, The University of Texas at Austin, May 1975.

Shirley, D. J., "Transducer for Generation and Detection of Shear Waves," ARL Invention Disclosure, September 1975.

Shirley, D. J., and A. L. Anderson, "In Situ Measurement of Marine Sediment Acoustical Properties During Coring in Deep Water," IEEE Trans. Geoscience Electronics GE-13, No. 4 (1975).

Shirley, D. J., and A. L. Anderson, "Acoustical and Engineering Properties of Sediments," Applied Research Laboratories Technical Report No. 75-58 (ARL-TR-75-58), Applied Research Laboratories, The University of Texas at Austin, October 1975.

Stokoe, K. H. (UT Austin), D. G. Anderson (Fugro, Inc.), E. J. Arnold (UT Austin), R. J. Hoar (UT Austin), and D. J. Shirley, "Proceedings of the 10th Annual Offshore Technology Conference, Houston, Texas, 8-11 May 1978.

Tucholke, B. E. (Lamont-Doherty Geological Observatory, Columbia University), and D. J. Shirley, "Comparison of Laboratory and In Situ Compressional-Wave Velocity Measurements on Sediment Cores from the Western North Atlantic," Journal of Geophysical Research, Vol. 84, No. B2, 687-695, 10 February 1979.

2 April 1980

DISTRIBUTION LIST FOR
ARL-TR-80-17
UNDER CONTRACT N00014-76-C-0117
UNCLASSIFIED

Copy No.

Commanding Officer
Naval Ocean Research and Development Activity
NSTL Station, MS 39529

1 Attn: R. R. Goodman (Code 110)
2 A. L. Anderson (Code 320)
3 S. Marshall (Code 340)
4 J. Paquin (Code 500)
5 R. Gardner (Code 520)
6 Code 530
7 J. Matthews (Code 362)

Commanding Officer
Office of Naval Research
Arlington, VA 22217

8 Attn: A. Sykes
9 T. Pyle (Code 48B)
10 H. Bezdek (Code 460)
11 M. Odegard (Code 48D)

Commanding Officer
Naval Electronic Systems Command
Department of the Navy
Washington, DC 20360

12 Attn: J. Sinsky (Code 320)
13 J. Reeves (Code PME 124-34)
14 H. Ford (Code PME 124-60)

Commander
Naval Sea Systems Command
Department of the Navy
Washington, DC 20362

15 Attn: A. P. Franceschetti

Chief of Naval Material
Department of the Navy
Washington, DC 20360

16 Attn: CAPT E. Young (Code 08724)

Distribution List for ARL-TR-80-17 under Contract N00014-76-C-0117

Copy No.

Commanding Officer
Naval Oceanographic Office
NSTL Station, MS 39529
17 Attn: W. Geddes
18 W. Jobst
19 M. G. Lewis

Commander
Naval Ocean Systems Center
Department of the Navy
San Diego, CA 92132
20 Attn: Library
21 M. A. Pedersen
22 N. O. Booth
23 E. L. Hamilton
24 H. P. Bucker

Director
Naval Research Laboratory
Department of the Navy
Washington, DC 20375
25 Attn: Code 2627
26 O. Diachok

Chief of Naval Operations
Department of the Navy
Washington, DC 20350
27 Attn: R. S. Winokur (OP-95E1)

Commander
Naval Air Development Center
Department of the Navy
Warminster, PA 18974
28 Attn: C. L. Bartberger

Commander
New London Laboratory
Naval Underwater Systems Center
Department of the Navy
New London, CT 06320
29 Attn: P. Herstein

Commanding Officer
Naval Coastal Systems Center
Panama City, FL 32401
30 Attn: E. G. McLeroy, Jr.
31 B. Tolbert

Distribution List for ARL-TR-80-17 under Contract N00014-76-C-0117

Copy No.

Superintendent
Naval Postgraduate School
Monterey, CA 93940
32 Attn: H. Medwin
33 Library

Woods Hole Oceanographic Institution
Woods Hole, MA 02543
34 Attn: C. Hollister
35 Dr. B. Tucholke

Hawaii Institute of Geophysics
The University of Hawaii
2525 Correa Road
Honolulu, HI 96822
36 Attn: Dr. G. Sutton
37 Dr. M. Manghnani

The Scripps Institution of Oceanography
The University of California/San Diego
San Diego, CA 92152
38 Attn: P. Lonsdale

Department of Geological Oceanography
Texas A&M University
College Station, TX 77840
39 Attn: Dr. W. R. Bryant

Underwater Systems, Inc.
3121 Georgia Avenue
Silver Spring, MD 20910
40 Attn: M. S. Weinstein

Geophysics Laboratory
Marine Science Institute
The University of Texas
700 The Strand
Galveston, TX 77550
41 Attn: Dr. G. Latham
42 Dr. E. W. Beherns

The Catholic University of America
6220 Michigan Avenue, NE
Washington, DC 20017
43 Attn: H. M. Überall

Lamont-Doherty Geological Observatory
Palisades, NY 10964
44 Attn: G. Bryan
45 W. J. Ludwig
46 R. D. Stoll

Distribution List for ARL-TR-80-17 under Contract N00014-76-C-0117

Copy No.

Department of Civil and Ocean Engineering
The University of Rhode Island
Kinston, RI 02881
47 Attn: Dr. A. J. Silva

University College of North Wales
Marine Science Laboratories
Menai Bridge
Anglesey, NORTH WALES
48 Attn: D. Taylor Smith
49 P. Schultheiss

Director
SACLANT ASW Research Centre
La Spezia, ITALY
50 Attn: T. Akal

The University of Auckland
Auckland, NEW ZEALAND
51 Attn: A. Kibblewhite, Department of Physics

Defence Research Establishment Pacific
CF Dockyard
Victoria, B. C., CANADA B2Y 327
52 Attn: Library

Defence Research Establishment Atlantic
9 Grove Street
Dartmouth, N. S., CANADA
53 Attn: Library

Department of Civil Engineering
The University of Texas at Austin
Austin, TX 78712
54 Attn: K. Stokoe

55 - 64 Commanding Officer and Director
Defense Technical Information Center
Cameron Station, Building 5
5010 Duke Street
Alexandria, VA 22314

Conoco, Inc.
Exploration Research
Drawer 1267
Ponca City, OK 74601
65 Attn: Dr. D. Bell
66 Dr. G. Brown

Distribution List for ARL-TR-80-17 under Contract N00014-76-C-0117

Copy No.

Southwest Research Institute
P. O. Drawer 28510
San Antonio, TX 78284
67 Attn: Dr. T. Owen

Electronics Research Laboratory
The University of Trondheim
The Norwegian Institute of Technology
O. S. Bragstad Plass 6
N-7034 Trondheim - NTH, NORWAY
68 Attn: Dr. J. Hovem

69 Office of Naval Research
Resident Representative
Room 582, Federal Building
Austin, TX 78701

70 Environmental Sciences Division, ARL:UT

71 David T. Blackstock, ARL:UT

72 Harlan G. Frey, ARL:UT

73 Loyd D. Hampton, ARL:UT

74 Kenneth E. Hawker, ARL:UT

75 S. K. Mitchell, ARL:UT

76 Thomas G. Muir, ARL:UT

77 Donald J. Shirley, ARL:UT

78 Reuben H. Wallace, ARL:UT

79 Library, ARL:UT

80 - 91 Reserve, ARL:UT